

AlphaNet: Improving Long-Tail Classification By Combining Classifiers

Nadine Chang^{1,*}
nchang1@cs.cmu.edu

Jayanth Koushik^{1,*}
jkoushik@andrew.cmu.edu

Aarti Singh¹
aartisingh@cmu.edu

Martial Hebert¹
hebert@cs.cmu.edu

Yu-Xiong Wang²
yxw@illinois.edu

Michael J. Tarr¹
michaeltarr@cmu.edu

Methods in long-tail learning focus on improving performance for data-poor (rare) classes; however, performance for such classes remains much lower than performance for more data-rich (frequent) classes. Analyzing the predictions of long-tail methods for rare classes reveals that a large number of errors are due to misclassification of rare items as visually similar frequent classes. To address this problem, we introduce AlphaNet, a method that can be applied to existing models, performing post hoc correction on classifiers of rare classes. Starting with a pre-trained model, we find frequent classes that are closest to rare classes in the model’s representation space and learn weights to update rare classifiers with a linear combination of frequent classifiers. AlphaNet, applied on several different models, greatly improves test accuracy for rare classes in multiple long-tail datasets. We then analyze predictions from AlphaNet and find that remaining errors are to often due to fine-grained differences among semantically similar classes (e.g., dog breeds). Evaluating with semantically similar classes grouped together, AlphaNet also improves overall accuracy, showing that the method is practical for long-tail classification problems.

1. Introduction

The significance of long-tailed distributions in real-world applications (such as autonomous driving^[1] and medical image analysis analysis^[2]) has spurred a variety of approaches for long-tail classification^[3]. Learning in this setting is challenging because many classes are “rare” – having only a small number of training samples. Some methods re-sample more data for rare classes in an effort to address data imbalances^[4,5], while other methods adjust learned classifiers to re-weight them in favor of rare classes^[6]. Both re-sampling and re-weighting methods provide strong baselines for long-tail clas-

sification tasks. However, state-of-the-art results are achieved by more complex methods that, for example, learn multiple experts^[7,8], perform multi-stage distillation^[9], or use a combination of weight balancing, data re-sampling, and loss decay^[10].

Despite these advances, accuracy on rare classes continues to be significantly worse than overall accuracy using these methods. For example, on the ImageNet-LT dataset, the 6-expert ensemble ‘routing diverse experts’ (RIDE) model^[7] has an average accuracy of 68.9% on frequent classes, but an average accuracy of 36.5% on rare classes. In addition to significantly reducing overall accuracy, such performance imbalances raise ethical concerns in contexts where unequal accuracy leads to biased outcomes, for instance in medical imaging^[11] or face detection^[12]. For example, models trained on chest X-rays consistently under-diagnosed minority groups^[13]. Similarly, cardiac image segmentation showed significant differences between racial groups^[14]. For these reasons, our method is aimed at directly improving the accuracy for rare classes in long-tail classification.

To understand the poor rare class performance of long-tail models, we analyzed the predictions of the RIDE model^[7] on ‘few’ split test samples – classes with limited training samples – in ImageNet-LT^[15]. Figure 1a shows predictions binned into three groups: 1) samples predicted correctly; 2) samples incorrectly predicted as a visually similar class (e.g., predicting ‘husky’ instead of ‘malamute’); and 3) samples incorrectly predicted as a visually dissimilar class (e.g., predicting ‘car’ instead of ‘malamute’). A significant portion of the misclassifications (about 26%) are to visually similar classes. Figure 1b shows samples from one pair of visually similar classes; the differences are subtle, and can be hard even for humans to identify. We next analyzed the relationship between per-class test accuracy and mean distance of a class to its nearest neighbors (see Section 3 for details). Figure 1c shows a strong positive correlation between accuracy and mean distance – ‘few’ split classes with close neighbors have lower test accuracy than classes with distant neighbors.

Based on these analyses, we introduce a method, AlphaNet, for improving classifiers for rare classes using information from visually similar *frequent* classes (Figure 2). At a high level, AlphaNet can be seen as moving the classifiers for

* Equal contribution. ¹ Carnegie Mellon University.

² University of Illinois Urbana-Champaign.

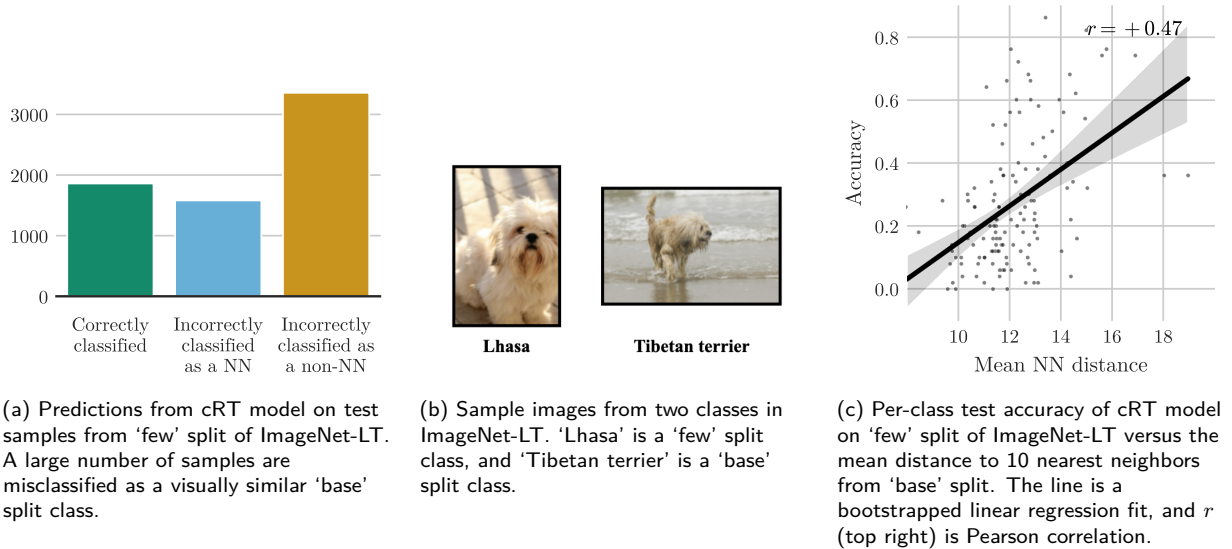


Figure 1: Analysis of test accuracy for 'few' split of ImageNet-LT.

rare classes based on their position relative to visually similar classes. Importantly, AlphaNet updates classifiers without making any changes to the representation space, or to other classifiers in the model. It performs a *post-hoc* correction, and as such, is applicable to use cases where existing base classifiers are either unavailable or fixed (e.g., due to commercial interests or data privacy protections). The simplicity of our method lends to computational advantages – AlphaNet can be trained rapidly, and on top of any classification model.

2. Related work

Combining, creating, modifying, and learning model weights are concepts that have been implemented in many earlier models. As we review below, these concepts appear frequently in, transfer learning, meta-learning, zero-shot/low-shot learning, and long-tail learning.

2.1. Classifier creation

The process of creating new classifiers is captured within meta-learning concepts such as learning-to-learn, transfer learning, and multi-task learning learning^[16,17,18,19,20]. These approaches generalize to novel tasks by learning shared information from a set of related tasks. Many studies find that shared information is embedded within model weights, and, thus, aim to learn structure within learned models to directly modify the weights of a different network^[21,22,23,24,25,26,27,28]. Other studies go even further and instead of modifying networks, they create entirely new networks exclusively from training samples samples^[29,30,31]. In contrast, AlphaNet only

combines existing classifiers, without having to create new classifiers or train networks from scratch.

2.2. Classifier or feature composition

In various classical approaches, there has been work that learns better embedding spaces for image annotation^[32], or uses classification scores as useful features^[33]. However, these approaches do not attempt to compose classifiers nor do they address the long-tail problem. Within non-deep methods in classic transfer learning, there have been attempts to use and combine support vector machines (SVMs). In one method^[34], SVMs are trained per object instance, and a hierarchical structure is required for combination in the datasets of interest. Such a structure is typically not guaranteed nor provided in long-tailed datasets. Another SVM method uses regularized minimization to learn the coefficients necessary to combine patches from other classifiers^[35].

While these approaches are conceptually similar to our method, AlphaNet has the additional advantage of *learning* the compositional coefficients without any hyper-parameters and tuning. Specifically, different novel classes will have their own sets of composition coefficients, and similar novel classes will naturally have similar coefficients. Learning such varying sets of coefficients is difficult in previous classical approaches, which either learn a fixed set of alphas for all novel classes or are forced to introduce more complex group sparsity-like constraints. Finally, in zero-shot learning there exist methods which compose classifiers of known visual concepts to learn a completely new classifier^[30,36,37,38]. However, such composition is often guided by additional attribute supervision or

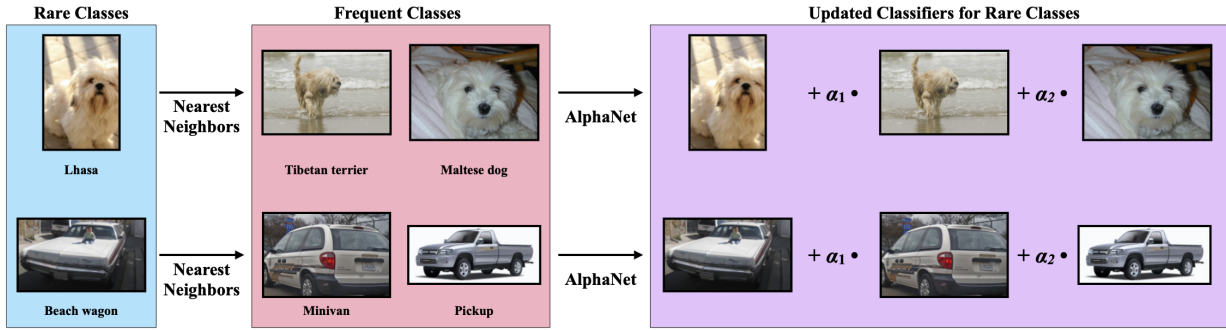


Figure 2: Pipeline for AlphaNet. Given examples from rare classes, we identify the nearest neighbors (visually similar) examples from frequent classes and then update each rare classifier using learned α 's for each nearest neighbor. The result is an improved classifier for each rare class.

textual description, which are not needed by AlphaNet.

2.3. Learning transformations between models and classes

Other studies have demonstrated different ways of learning transformations to modify model weights in an attempt to learn these transformations with stochastic gradient descent (SGD) optimization^[39,40]. Additionally, there is empirical evidence^[41] showing the existence of a generic nonlinear transformation from small-sample to large-sample models for different types of feature spaces and classifier models. Finally, in the case where one learns the transformation from the source function to a related target function, there are theoretical guarantees on performance^[42]. AlphaNet is similar in that we likewise infer that our target classifier is a transformation from a set of source classifiers.

2.4. Zero-shot/low-shot learning

Meta-learning, transfer learning, and learning-to-learn are frequently applied to the domain of low-shot learning^[20,41,43,44,45,46,47,48,49,50,51,52]. A wide variety of prior studies have attempted to transfer knowledge from tasks with abundant data to completely novel tasks^[23,40,53]. However, the explicit nature of low-shot learning consisting of tasks with small fixed samples means that these approaches do not generalize well beyond the arbitrary few tasks. This is a significant problem as the visual world clearly involves a wide set of tasks with continuously varying amounts of information.

2.5. Long-tail learning

The restrictions of low-shot learning have directly led to the new paradigm referred to as long-tail learning, where data samples are continuously decreasing and the data distribu-

tion closely models that of the visual world. Recent work achieves state-of-the-art performance on long-tailed recognition by learning multiple experts^[7,8]. Both of these complex ensemble methods require a two-stage training method. A somewhat different approach re-balances the samples at different stages of model training^[5], attempts to transfer features from common classes to rare classes^[15], or transfers intra-class variance^[54]. However, approaches to knowledge transfer require complex architectures, such as a specialized attention mechanism and memory models^[15]. While most studies have largely focused on representation space transferability or complex ensembles, recent work establishes a strong baseline by exploring the potential of operating in classifier space^[6]. Results suggest that decoupling model representation learning and classifier learning is a more efficient way to approach long-tailed learning. Specifically, methods normalizing classifiers and adjusting classifiers only using re-sampling strategies achieve good performance. Such successes in working only with classifiers support our general concept that combining strong classifiers in AlphaNet is a natural and direct way to improve upon weak classifiers.

3. Methods

3.1. Notation

In this work, we will define the distance between two classes as the distance between their average training set representation. Given a classification model, let f be the function mapping images to vectors in \mathbb{R}^d (typically, this is the output of the penultimate layer in convolutional networks). For a class c with training samples $I_1^c, \dots, I_{n^c}^c$, let $z^c \equiv (1/n^c) \sum_i f(I_i^c)$. Given a distance metric $\mu : \mathbb{R}^d \times \mathbb{R}^d \rightarrow \mathbb{R}$, for classes c_1 and c_2 , we define $m_\mu(c_1, c_2) \equiv \mu(x^{c_1}, x^{c_2})$.

Given a long-tailed dataset, the ‘few’ split, C^F , is defined as the set of rare classes (which form the “tail” of the training data distribution). The set of remaining classes forms the ‘base’ split, C^B . AlphaNet is applied to update the ‘few’ split classifiers using nearest neighbors from the ‘base’ split. For a ‘few’ split class c , let the k nearest ‘base’ split neighbors (based on m_μ) be q_1^c, \dots, q_k^c .

We will use the term ‘classifier’ to denote the linear mapping from feature vectors to class scores. In convolutional networks, the last layer is generally a matrix of all individual classifiers. For a class c , let w^c be its classifier, and let v_1^c, \dots, v_k^c be the classifiers for its nearest neighbors. Finally, let $\bar{v}^c \in \mathbb{R}^{kd}$ be a vector with the nearest neighbor classifiers concatenated together.

3.2. AlphaNet implementation

Figure 2 shows the architecture of our method. AlphaNet is a small fully connected network which maps \bar{v}^c to a set of coefficients $\alpha_1^c, \dots, \alpha_k^c$. The α coefficients (denoted together as a vector α^c), are then scaled to unit 1-norm (the reasoning behind this is explained below):

$$\tilde{\alpha}^c = \alpha^c / |\alpha^c|_1. \quad (1)$$

The scaled coefficients are used to update classifiers through a linear combination:

$$\hat{w}^c \equiv w^c + \sum_{i=1}^k \tilde{\alpha}_i^c v_i^c \quad (2)$$

Due to the 1-norm scaling, we have

$$\begin{aligned} \|\hat{w}^c - w^c\|_2 &\leq \sum_{i=1}^k |\tilde{\alpha}_i^c| \|v_i^c\|_2 \quad (\text{Cauchy-Schwarz inequality}) \\ &\leq \max_{i=1, \dots, k} \|v_i^c\|_2 \sum_{i=1}^k |\tilde{\alpha}_i^c| \\ &= \max_{i=1, \dots, k} \|v_i^c\|_2 \|\tilde{\alpha}^c\|_1 \\ &= \max_{i=1, \dots, k} \|v_i^c\|_2, \end{aligned} \quad (3)$$

that is, a classifier’s change is bound by the norm of its class’s nearest neighbors. Thanks to this, we do not need to update or rescale ‘base’ split classifiers, which may not be possible in certain domains.

A single network is used to generate coefficients for every ‘few’ split class. So, once trained, AlphaNet can be applied even to previously unseen classes.

3.3. Training

To train AlphaNet, we have to learn parameters θ for the network which maps \bar{v}^c to α^c . We also learn a new set of

bias values for the ‘few’ split classes, $\tilde{b}_1, \dots, \tilde{b}_{|C^F|}$. We train AlphaNet using samples from both the ‘few’ and ‘base’ splits to prevent over-fitting. So, for a sample (I, y) , the prediction score is given by

$$s(I, y; \theta, \tilde{b}) = \begin{cases} f(I)^T \hat{w}^y + \tilde{b}_y & y \in C^F \\ f(I)^T w^y + b_y & y \in C^B \end{cases} \quad (4)$$

This score is used to compute the softmax cross-entropy loss on a set of training samples, and minimized with respect to θ and \tilde{b} using SGD.

4. Experiments

4.1. Experimental setup

Datasets. We evaluated our method using three long-tailed datasets: ImageNet-LT, Places-LT^[15], and CIFAR-100-LT^[10]. These Datasets are sampled from their respective original datasets, ImageNet^[55], Places365^[56], and CIFAR-100^[57] such that the new distributions follow a standard long-tailed distribution. For CIFAR-100-LT, we used an imbalance factor of 100.

The datasets are broken down into three broad splits that indicate the number of training samples per class: 1) ‘many’ contains classes with greater than 100 samples; 2) ‘medium’ contains classes with greater than or equal to 20 samples but less than or equal to 100 samples; 3) ‘few’ contains classes with less than 20 samples. The test set is always balanced, containing an equal number of samples for each class. We use the term ‘base’ split to refer to the combined ‘many’ and ‘medium’ splits.

Note: Another popular dataset used for testing long-tail models is iNaturalist^[58]. Results for this dataset, however, are much more balanced across splits. So it does not represent a valid use case for our proposed method, and we omitted the dataset from our experiments.

Training data sampling. In order to prevent over-fitting on the ‘few’ split samples, we used a class balanced sampling approach, using all ‘few’ split samples, and a portion of the ‘base’ split samples. Given F ‘few’ split samples, and a ratio ρ , every epoch, ρF samples were drawn from the ‘base’ split, with sample weights inversely proportional to the class size. This ensured that all ‘base’ classes had an equal probability of being sampled. As we show in the following section, ρ allows us to control the balance between ‘few’ and ‘base’ split accuracy. We evaluated AlphaNet with a range of ρ values; results for $\rho = 0.5$, $\rho = 1$, and $\rho = 1.5$ are shown in the following section, and the full set of results is in the appendix.

Training. All experiments used an AlphaNet module with three 32 unit layers, and Leaky-ReLU activation^[59]. Unless stated otherwise, euclidean distance was used to find $k = 5$ nearest neighbors for each ‘few’ split class. Models

were trained for 25 epochs to minimize cross-entropy loss computed using mini-batches of 64 samples. Optimization was performed using AdamW^[60] with a learning rate of 0.001, decayed by a factor of 10, every 10 epochs. Model weights were saved after each epoch, and after training, the weights with the best accuracy on validation data were used to report results on the test set. All experiments were repeated 10 times, and we report mean and standard deviation of accuracies across trials.

4.2. Long-tail classification results

Method	Few	Med.	Many	Overall
ImageNet-LT				
Cross entropy	7.7	37.5	65.9	44.4
NCM	28.1	45.3	56.6	47.3
τ -normalized	30.7	46.9	59.1	49.4
cRT	27.4	46.2	61.8	49.6
α -cRT ($\rho = 0.5$)	39.71 ^{.42}	42.0 ^{.66}	58.30 ^{.52}	48.0 ^{.37}
α -cRT ($\rho = 1$)	34.61 ^{.88}	43.70 ^{.51}	59.70 ^{.43}	48.6 ^{.24}
α -cRT ($\rho = 1.5$)	32.62 ^{.46}	44.40 ^{.49}	60.30 ^{.38}	48.90 ^{.19}
LWS	30.4	47.2	60.2	49.9
α -LWS ($\rho = 0.5$)	46.99 ^{.98}	38.60 ^{.87}	52.90 ^{.86}	45.30 ^{.69}
α -LWS ($\rho = 1$)	41.61 ^{.61}	42.20 ^{.53}	56.00 ^{.32}	47.40 ^{.30}
α -LWS ($\rho = 1.5$)	40.11 ^{.99}	43.20 ^{.98}	56.90 ^{.76}	48.00 ^{.53}
Places-LT				
Cross entropy	8.2	27.3	45.7	30.2
NCM	27.3	37.1	40.4	36.4
τ -normalized	31.8	40.7	37.8	37.9
cRT	24.9	37.6	42.0	36.7
α -cRT ($\rho = 0.5$)	31.09 ^{.88}	34.50 ^{.17}	40.40 ^{.29}	35.90 ^{.09}
α -cRT ($\rho = 1$)	27.01 ^{.02}	36.10 ^{.31}	41.30 ^{.13}	36.20 ^{.10}
α -cRT ($\rho = 1.5$)	25.50 ^{.89}	36.50 ^{.36}	41.60 ^{.21}	36.20 ^{.11}
LWS	28.7	39.1	40.6	37.6
α -LWS ($\rho = 0.5$)	37.11 ^{.39}	34.40 ^{.80}	37.70 ^{.52}	36.10 ^{.31}
α -LWS ($\rho = 1$)	34.60 ^{.97}	35.80 ^{.54}	38.60 ^{.39}	36.60 ^{.22}
α -LWS ($\rho = 1.5$)	32.21 ^{.17}	37.20 ^{.36}	39.50 ^{.39}	37.00 ^{.11}

Table 1: Mean split accuracy (standard deviation in super-script) of AlphaNet and various baseline methods on ImageNet-LT and Places-LT. α classifier re-training (cRT) and α learnable weight scaling (LWS) are AlphaNet models applied over cRT and LWS features respectively.

Baseline models. First, we applied AlphaNet on several strong baseline methods^[6]. These methods have good overall accuracy, but accuracy for ‘few’ split classes is much lower. On the ImageNet-LT dataset, average accuracy for the cRT and LWS models (using a ResNeXt-50 backbone) is nearly 20 points below the overall accuracy, as seen in Table 1. Using features extracted from these two models, we used AlphaNet

to update ‘few’ split classifiers. On both models, we saw a significant increase in the ‘few’ split accuracy for all values of ρ . For $\rho = 1$, average ‘few’ split accuracy was boosted by 7 points for the cRT model, and about 11 points for the LWS model.

We repeated the above experiment on the Places-LT dataset, where again ‘few’ split accuracy for the cRT and LWS models is much lower than the overall accuracy (by around 12 and 9 points respectively as seen in Table 1. With $\rho = 1$, AlphaNet improved ‘few’ split accuracy by 2 points on average for the cRT model, and about 6 points on average for the LWS model.

Method	Few	Med.	Many	Overall
ImageNet-LT				
RIDE	36.5	54.4	68.9	57.5
α -RIDE ($\rho = 0.5$)	43.50 ^{.75}	52.30 ^{.26}	67.30 ^{.17}	56.90 ^{.11}
α -RIDE ($\rho = 1$)	40.81 ^{.00}	53.10 ^{.21}	67.90 ^{.18}	57.10 ^{.11}
α -RIDE ($\rho = 1.5$)	38.21 ^{.22}	53.60 ^{.25}	68.40 ^{.17}	57.20 ^{.06}
CIFAR-100-LT				
RIDE	25.8	52.1	69.3	50.2
α -RIDE ($\rho = 0.5$)	30.91 ^{.82}	47.01 ^{.25}	65.70 ^{.94}	48.70 ^{.41}
α -RIDE ($\rho = 1$)	27.21 ^{.69}	49.10 ^{.85}	67.40 ^{.62}	48.90 ^{.30}
α -RIDE ($\rho = 1.5$)	25.01 ^{.15}	50.11 ^{.12}	67.91 ^{.01}	48.80 ^{.63}

Table 2: Mean split accuracy (standard deviation in super-script) on ImageNet-LT and CIFAR-100-LT using the ensemble RIDE model^[7]. α RIDE applies AlphaNet on average features from the ensemble.

Expert model. Next, we applied AlphaNet on the 6-expert ensemble RIDE model^[7]. We provided the combined feature vectors from all 6 experts as input to AlphaNet. The learned ‘few’ split classifiers were split into 6, and used to update the experts. Prediction scores from the experts were averaged to produce the final predictions, as in the original model. For ImageNet-LT, the experts used a ResNeXt-50 backbone, and for CIFAR-100-LT, a ResNet-32 backbone. Table 2 shows the base results for the expert models, along with AlphaNet results for $\rho = 0.5, 1, 2$. On ImageNet-LT, ‘few’ split accuracy was increased by up to 7 points, and on CIFAR-100-LT, by 5 points.

4.3. Comparison with control

Our method is based on the core hypothesis that classifiers can be improved using nearest neighbors. In this section, we directly test this hypothesis. Based on the results in the previous section, the improvements in ‘few’ split accuracy could be attributed simply to the extra fine-tuning of ‘few’ split classifiers. So, we repeated the experiments of the previous section with randomly chosen neighbors for each ‘few’ split class, rather than nearest neighbors. This differs from our

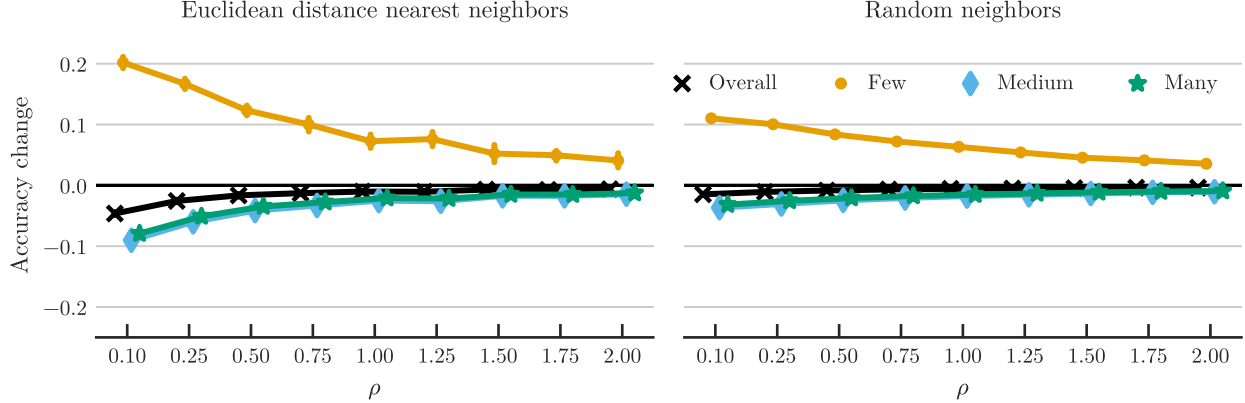


Figure 3: Change in split accuracy for AlphaNet training of cRT model on ImageNet-LT. For each value of ρ , the two plots show the change in split accuracy for AlphaNet compared to the baseline cRT model, as well as the change in overall accuracy. Left shows the results for normal training with 5 euclidean nearest neighbors, and right shows the results for training with 5 random neighbors for each ‘few’ split class. Training with nearest neighbors leads to a larger increase in ‘few’ split accuracy (especially for small values of ρ), which cannot be accounted for by the additional fine-tuning of classifiers.

previous experiments only in the nature of neighbors used, so if our method’s improvements are solely due to extra fine-tuning, we should see the same results. However, as seen in Figure 3, training with nearest neighbors garners much larger improvements in ‘few’ split accuracy, with similar trends in overall accuracy. This supports our hypothesis that data-poor classes can make use of information from neighbors to improve classification performance.

4.4. Prediction changes

As shown in Section 1, the cRT model frequently misclassifies ‘few’ split classes as visually similar ‘base’ split classes. Using the AlphaNet model with $\rho = 0.5$, we performed the same analyses as before. Figure 5a shows the change in sample predictions. A large portion of samples previously misclassified as a nearest neighbor are correctly classified after their classes are updated with AlphaNet. Furthermore, as seen in Figure 4, AlphaNet improvements are strongly correlated to mean nearest neighbor distance. Classes with close neighbors, which had a high likelihood of being misclassified by the baseline model, see the biggest improvement in test accuracy.

4.5. Analysis of AlphaNet predictions

AlphaNet significantly boosts the accuracy of ‘few’ split classes. However, looking at Table 1 and Table 2, we see that the overall accuracy decreases compared to baseline models, particularly for small values of ρ . It is important to note that the increase in ‘few’ split accuracy is much larger than the decrease in overall accuracy. As discussed earlier, in many applications it is important to have balanced performance across classes, and AlphaNet succeeds in making accuracies

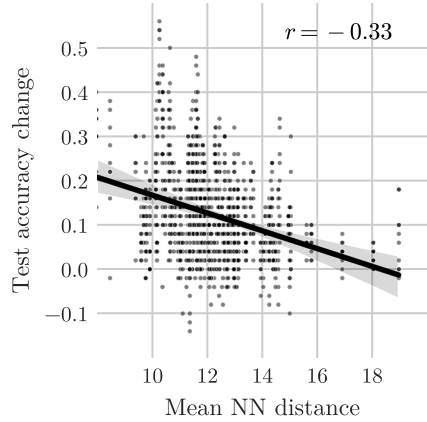
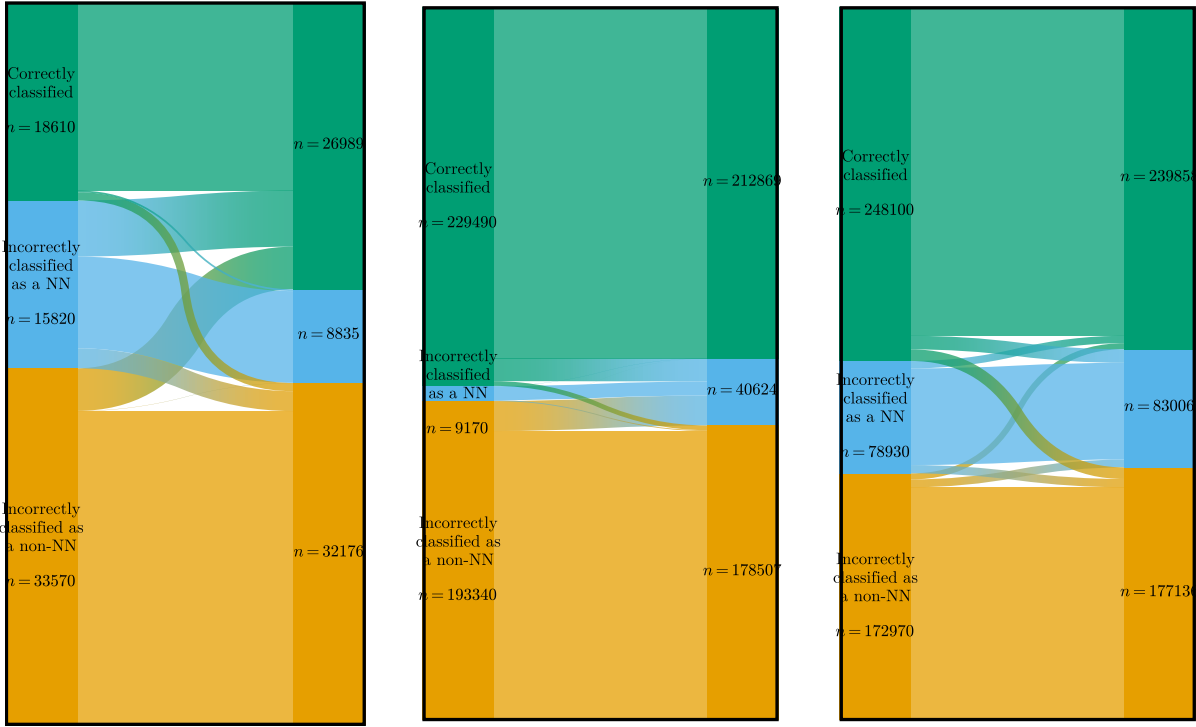


Figure 4: Change in per-class accuracy for AlphaNet applied over cRT features, versus mean Euclidean distance to five nearest neighbors. Comparing with Figure 1c, we can see that AlphaNet provides the largest boost to classes with poor baseline performance, which have close nearest neighbors.

more balanced across splits.

However, we further analyzed the prediction changes for ‘base’ split samples. Specifically, Figure 5b shows change in predictions for ‘base’ split samples, with nearest neighbors selected from the ‘few’ split. We see a small increase in misclassifications as ‘few’ split classes. This leads to the slight decrease in overall accuracy, which is also evident in Figure 5c where all predictions are shown, and with nearest neighbors from all classes.

The previous analysis was conducted using nearest neigh-



(a) Predictions on ‘few’ split classes, with nearest neighbors selected from ‘base’ split classes.

(b) Predictions on ‘base’ split classes, with nearest neighbors selected from ‘few’ split classes.

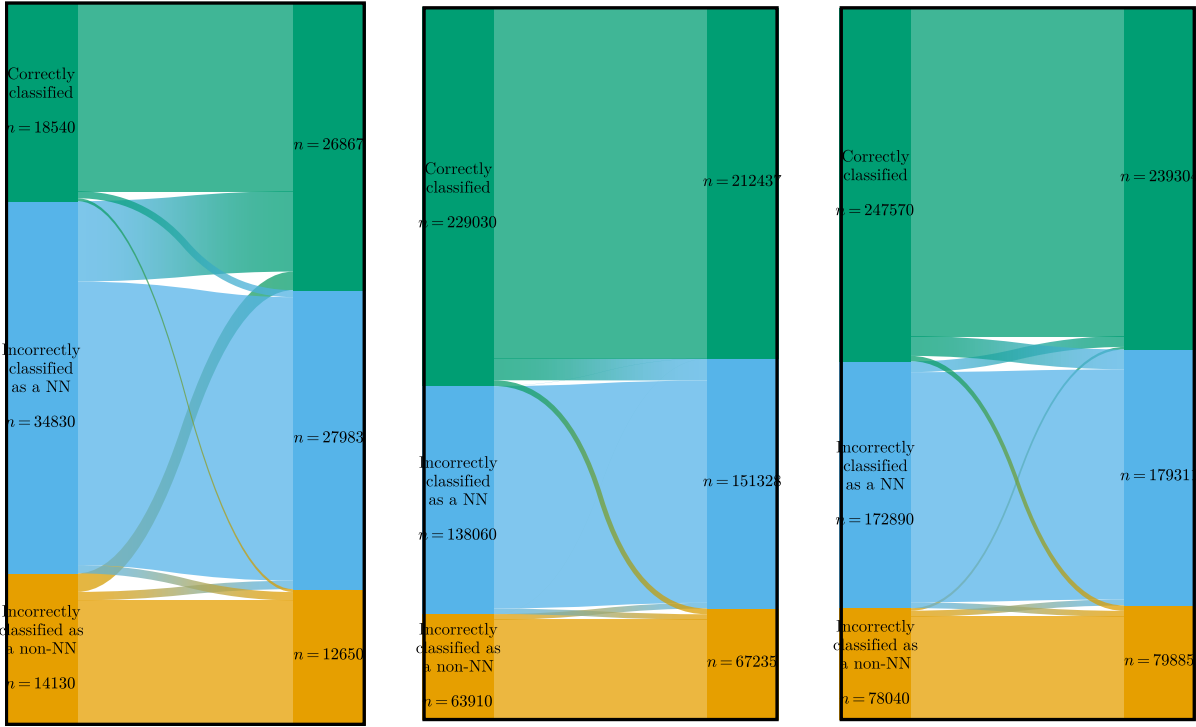
(c) All predictions, with nearest neighbors selected from all classes.

Figure 5: Change in sample predictions for AlphaNet applied for cRT features, with $k = 10$ nearest neighbors by Euclidean distance. The bars on the left show the distribution of predictions by the baseline model; and the bars on the right show the distribution for AlphaNet. The counts are aggregated from 10 different runs of AlphaNet. The “flow” bands from left to right show the changes in individual sample predictions.

bors identified based on visual similarity. Since this is dependent on the particular model, we conducted an additional analysis to see the behavior of predictions with respect to *semantically similar* categories. For classes in ImageNet-LT, we defined nearest neighbors using distance in the WordNet hierarchy. Specifically, if two classes (e.g., ‘Lhasa’ and ‘Tibetan terrier’) share a parent at most four levels higher in WordNet (in this example, ‘dog’), we consider them to be nearest neighbors. Figure 6 shows the predictions for AlphaNet with cRT grouped based on these nearest neighbors. As we can see, a large number of predictions which are considered incorrect are among semantically similar categories which can be hard for even humans to distinguish. This suggests that metrics for long-tail classification might need to be re-evaluated for large datasets with many similar classes.

5. Conclusion

The long-tailed nature of the world presents a challenge for any model that depends on learning over specific examples. Most long-tailed methods tend to have high overall accuracy, but with unbalanced accuracies where frequent classes are learned well with high accuracies and rare classes are learned poorly with low accuracies. As such, the long-tailed world represents one source of potential bias^[11]. To address this problem, typical approaches resort to re-sampling or re-weighting of rare classes but still focus on achieving the highest overall accuracy. Consequently, these methods continue to suffer from low accuracy for data-poor classes, and an accuracy imbalance across data-rich and data-poor classes. In contrast, our method, AlphaNet, provides a rapid 5 minute *post-hoc* correction that can sit on top of any model using classifiers. This simple method greatly improves the accuracy for data-poor classes, and re-balances classification accuracy in a way



(a) Predictions on ‘few’ split classes, with nearest neighbors selected from ‘base’ split classes.

(b) Predictions on ‘base’ split classes, with nearest neighbors selected from ‘few’ split classes.

(c) All predictions, with nearest neighbors selected from all classes.

Figure 6: Change in sample predictions for AlphaNet applied for CRT features, with nearest neighbors identified using WordNet categories. This figure represents the same predictions as Figure 5, but grouped differently.

that overall classification accuracy is preserved. In addition to directly addressing training imbalances, AlphaNet is also applicable to re-balancing accuracies across biases arising from model structure or the prioritization of different model parameters. We analyzed the predictions of our model, and showed that when considering semantically similar classes together, AlphaNet achieves accuracy on par with baselines, while also improving accuracy for data-poor classes significantly. AlphaNet is deployable in any application where the base classifiers cannot be changed, but balanced performance is desirable – thereby making it useful in contexts where ethics, privacy, or intellectual property are concerns.

References

- [1] Athma Narayanan, Yi-Ting Chen, and Srikanth Malla. Semi-supervised learning: Fusion of self-supervised, supervised learning, and multimodal cues for tactical driver behavior detection. *arXiv preprint arXiv:1807.00864*, 2018.
- [2] Zhixiong Yang, Junwen Pan, Yanzhan Yang, Xiaozhou Shi, Hong-Yu Zhou, Zhicheng Zhang, and Cheng Bian. Proco: Prototype-aware contrastive learning for long-tailed medical image classification. In *Medical Image Computing and Computer Assisted Intervention–MICCAI 2022: 25th International Conference, Singapore, September 18–22, 2022, Proceedings, Part VIII*, pages 173–182. Springer, 2022.
- [3] Lu Yang, He Jiang, Qing Song, and Jun Guo. A survey on long-tailed visual recognition. *International Journal of Computer Vision*, 130(7):1837–1872, 2022.
- [4] Yin Cui, Menglin Jia, Tsung-Yi Lin, Yang Song, and Serge Belongie. Class-balanced loss based on effective number of samples. *2019 IEEE/CVF Conference on Computer Vision and Pattern Recognition (CVPR)*, 00:9260–9269, 2019. doi: 10.1109/cvpr.2019.00949.
- [5] Kaidi Cao, Colin Wei, Adrien Gaidon, Nikos Arechiga, and Tengyu Ma. Learning imbalanced datasets with label-distribution-aware margin loss. *arXiv*, 2019. doi: 10.48550/arxiv.1906.07413.
- [6] Bingyi Kang, Saining Xie, Marcus Rohrbach, Zhicheng Yan, Albert Gordo, Jiashi Feng, and Yannis Kalantidis. Decoupling representation and classifier for long-tailed recognition. *arXiv*, 2019.
- [7] Xudong Wang, Long Lian, Zhongqi Miao, Ziwei Liu, and Stella X Yu. Long-tailed recognition by routing diverse distribution-aware experts. *arXiv*, 2020. doi: 10.48550/arxiv.2010.01809.

- [8] Jiarui Cai, Yizhou Wang, and Jenq-Neng Hwang. Ace: Ally complementary experts for solving long-tailed recognition in one-shot. *2021 IEEE/CVF International Conference on Computer Vision (ICCV)*, 00: 112–121, 2021. doi: 10.1109/iccv48922.2021.00018.
- [9] Tianhao Li, Limin Wang, and Gangshan Wu. Self supervision to distillation for long-tailed visual recognition. *arXiv*, 2021. doi: 10.48550/arxiv.2109.04075.
- [10] Shaden Alshammari, Yu-Xiong Wang, Deva Ramanan, and Shu Kong. Long-tailed recognition via weight balancing. *2022 IEEE/CVF Conference on Computer Vision and Pattern Recognition (CVPR)*, 00: 6887–6897, 2022. doi: 10.1109/cvpr52688.2022.00677.
- [11] María Agustina Ricci Lara, Rodrigo Echeveste, and Enzo Ferante. Addressing fairness in artificial intelligence for medical imaging. *Nature Communications*, 13(1):4581, 2022. doi: 10.1038/s41467-022-32186-3.
- [12] Joy Buolamwini and Timnit Gebru. Gender shades: Intersectional accuracy disparities in commercial gender classification. In *Conference on fairness, accountability and transparency*, pages 77–91. PMLR, 2018.
- [13] Laleh Seyyed-Kalantari, Haoran Zhang, Matthew BA McDermott, Irene Y Chen, and Marzyeh Ghassemi. Underdiagnosis bias of artificial intelligence algorithms applied to chest radiographs in under-served patient populations. *Nature medicine*, 27(12):2176–2182, 2021.
- [14] Esther Puyol-Antón, Bram Ruijsink, Stefan K Piechnik, Stefan Neubauer, Steffen E Petersen, Reza Razavi, and Andrew P King. Fairness in cardiac mr image analysis: an investigation of bias due to data imbalance in deep learning based segmentation. In *Medical Image Computing and Computer Assisted Intervention—MICCAI 2021: 24th International Conference, Strasbourg, France, September 27–October 1, 2021, Proceedings, Part III 24*, pages 413–423. Springer, 2021.
- [15] Ziwei Liu, Zhongqi Miao, Xiaohang Zhan, Jiayun Wang, Boqing Gong, and Stella X. Yu. Large-scale long-tailed recognition in an open world. *2019 IEEE/CVF Conference on Computer Vision and Pattern Recognition (CVPR)*, 00:2532–2541, 2019. doi: 10.1109/cvpr.2019.00264.
- [16] Sebastian Thrun. *Lifelong Learning Algorithms*, chapter 8, pages 181–209. Springer, 1998. doi: 10.1007/978-1-4615-5529-2_8.
- [17] Jürgen Schmidhuber, Jieyu Zhao, and Marco Wiering. Shifting inductive bias with success-story algorithm, adaptive Levin search, and incremental self-improvement. *Machine Learning*, 28(1):105–130, 1997. ISSN 0885-6125. doi: 10.1023/a:1007383707642.
- [18] Sinno Jialin Pan and Qiang Yang. A survey on transfer learning. *IEEE Transactions on Knowledge and Data Engineering*, 22(10):1345–1359, 2009. ISSN 1041-4347. doi: 10.1109/tkde.2009.191.
- [19] Rich Caruana. Multitask learning. *Machine Learning*, 28(1):41–75, 1997. ISSN 0885-6125. doi: 10.1023/a:1007379606734.
- [20] Adam Santoro, Sergey Bartunov, Matthew Botvinick, Daan Wierstra, and Timothy Lillicrap. One-shot learning with memory-augmented neural networks. *arXiv*, 2016. doi: 10.48550/arxiv.1605.06065.
- [21] J. Schmidhuber. A neural network that embeds its own meta-levels. *IEEE International Conference on Neural Networks*, pages 407–412 vol.1, 1993. doi: 10.1109/icnn.1993.298591.
- [22] Jrgen Schmidhuber. Learning to control fast-weight memories: An alternative to dynamic recurrent networks. *Neural Computation*, 4(1): 131–139, 1992. ISSN 0899-7667. doi: 10.1162/neco.1992.4.1.131.
- [23] Luca Bertinetto, João F Henriques, Jack Valmadre, Philip H S Torr, and Andrea Vedaldi. Learning feed-forward one-shot learners. *arXiv*, 2016. doi: 10.48550/arxiv.1606.05233.
- [24] David Ha, Andrew Dai, and Quoc V Le. Hypernetworks. *arXiv*, 2016. doi: 10.48550/arxiv.1609.09106.
- [25] Chelsea Finn, Kelvin Xu, and Sergey Levine. Probabilistic model-agnostic meta-learning. *arXiv*, 2018. doi: 10.48550/arxiv.1806.02817.
- [26] Sylvestre-Alvise Rebuffi, Hakan Bilen, and Andrea Vedaldi. Learning multiple visual domains with residual adapters. *arXiv*, 2017. doi: 10.48550/arxiv.1705.08045.
- [27] Abhishek Sinha, Mausoom Sarkar, Aahitagni Mukherjee, and Balaji Krishnamurthy. Introspection: Accelerating neural network training by learning weight evolution. *arXiv*, 2017. doi: 10.48550/arxiv.1704.04959.
- [28] Tsendsuren Munkhdalai and Hong Yu. Meta networks. *Proceedings of machine learning research*, 70:2554–2563, 2017.
- [29] Richard Socher, Milind Ganjoo, Hamsa Sridhar, Osbert Bastani, Christopher D Manning, and Andrew Y Ng. Zero-shot learning through cross-modal transfer. *arXiv*, 2013. doi: 10.48550/arxiv.1301.3666.
- [30] Jimmy Lei Ba, Kevin Swersky, Sanja Fidler, and Ruslan Salakhutdinov. Predicting deep zero-shot convolutional neural networks using textual descriptions. *2015 IEEE International Conference on Computer Vision (ICCV)*, pages 4247–4255, 2015. doi: 10.1109/iccv.2015.483.
- [31] Hyeonwoo Noh, Paul Hongseok Seo, and Bohyung Han. Image question answering using convolutional neural network with dynamic parameter prediction. *2016 IEEE Conference on Computer Vision and Pattern Recognition (CVPR)*, pages 30–38, 2016. doi: 10.1109/cvpr.2016.11.
- [32] Jason Weston, Samy Bengio, and Nicolas Usunier. Large scale image annotation: learning to rank with joint word-image embeddings. *Machine Learning*, 81(1):21–35, 2010. ISSN 0885-6125. doi: 10.1007/s10994-010-5198-3.
- [33] Gang Wang, Derek Hoiem, and David Forsyth. Learning image similarity from flickr groups using fast kernel machines. *IEEE Transactions on Pattern Analysis and Machine Intelligence*, 34(11):2177–2188, 2012. ISSN 0162-8828. doi: 10.1109/tpami.2012.29.
- [34] Ioannis Tsochantaridis, Thorsten Joachims, Thomas Hofmann, Yasemin Altun, and Yoram Singer. Large margin methods for structured and interdependent output variables. *Journal of machine learning research*, 6(9), 2005.
- [35] Yusuf Aytar and Andrew Zisserman. Enhancing exemplar svms using part level transfer regularization. *Proceedings of the British Machine Vision Conference 2012*, pages 79.1–79.11, 2012. doi: 10.5244/c.26.79.
- [36] Mohamed Elhoseiny, Babak Saleh, and Ahmed Elgammal. Write a classifier: Zero-shot learning using purely textual descriptions. *2013 IEEE International Conference on Computer Vision*, pages 2584–2591, 2013. doi: 10.1109/iccv.2013.321.
- [37] Ishan Misra, Abhinav Gupta, and Martial Hebert. From red wine to red tomato: Composition with context. *2017 IEEE Conference on Computer Vision and Pattern Recognition (CVPR)*, pages 1160–1169, 2017. doi: 10.1109/cvpr.2017.129.
- [38] Soravit Changpinyo, Wei-Lun Chao, Boqing Gong, and Fei Sha. Synthesized classifiers for zero-shot learning. *2016 IEEE Conference on Computer Vision and Pattern Recognition (CVPR)*, pages 5327–5336, 2016. doi: 10.1109/cvpr.2016.575.

- [39] Marcin Andrychowicz, Misha Denil, Sergio Gomez, Matthew W Hoffman, David Pfau, Tom Schaul, Brendan Shillingford, and Nando de Freitas. Learning to learn by gradient descent by gradient descent. *arXiv*, 2016. doi: 10.48550/arxiv.1606.04474.
- [40] Sachin Ravi and Hugo Larochelle. Optimization as a model for few-shot learning. In *International conference on learning representations*, 2017.
- [41] Yu-Xiong Wang and Martial Hebert. Computer vision – eccv 2016, 14th european conference, amsterdam, the netherlands, october 11–14, 2016, proceedings, part vi. *Lecture Notes in Computer Science*, pages 616–634, 2016. ISSN 0302-9743. doi: 10.1007/978-3-319-46466-4_37.
- [42] Simon Shaolei Du, Jayanth Koushik, Aarti Singh, and Barnabas Poczos. Hypothesis transfer learning via transformation functions. *arXiv*, 2016. doi: 10.48550/arxiv.1612.01020.
- [43] Li Fei-Fei, Rob Fergus, and Pietro Perona. One-shot learning of object categories. *IEEE Transactions on Pattern Analysis and Machine Intelligence*, 28(4):594–611, 2006. ISSN 0162-8828. doi: 10.1109/tpami.2006.79.
- [44] Gregory Koch, Richard Zemel, Ruslan Salakhutdinov, et al. Siamese neural networks for one-shot image recognition. In *ICML deep learning workshop*, volume 2. Lille, 2015.
- [45] Brenden M. Lake, Ruslan Salakhutdinov, and Joshua B. Tenenbaum. Human-level concept learning through probabilistic program induction. *Science*, 350(6266):1332–1338, 2015. ISSN 0036-8075. doi: 10.1126/science.aab3050.
- [46] Zhizhong Li and Derek Hoiem. Learning without forgetting. *arXiv*, 2016. doi: 10.48550/arxiv.1606.09282.
- [47] Bharath Hariharan and Ross Girshick. Low-shot visual recognition by shrinking and hallucinating features. *2017 IEEE International Conference on Computer Vision (ICCV)*, pages 3037–3046, 2017. doi: 10.1109/iccv.2017.328.
- [48] Jane Bromley, Isabelle Guyon, Yann LeCun, Eduard Säckinger, and Roopak Shah. Signature verification using a “siamese” time delay neural network. *Advances in neural information processing systems*, 6, 1993.
- [49] Jake Snell, Kevin Swersky, and Richard S Zemel. Prototypical networks for few-shot learning. *arXiv*, 2017. doi: 10.48550/arxiv.1703.05175.
- [50] Dileep George, Wolfgang Lehrach, Ken Kansky, Miguel Lázaro-Gredilla, Christopher Laan, Bhaskara Marthi, Xinghua Lou, Zhaoshi Meng, Yi Liu, Huayan Wang, Alex Lavin, and D. Scott Phoenix. A generative vision model that trains with high data efficiency and breaks text-based captchas. *Science*, 358(6368), 2017. ISSN 0036-8075. doi: 10.1126/science.aag2612.
- [51] Yu-Xiong Wang, Deva Ramanan, and Martial Hebert. Learning to model the tail. *Advances in neural information processing systems*, 30, 2017.
- [52] Zeynep Akata, Florent Perronnin, Zaid Harchaoui, and Cordelia Schmid. Label-embedding for image classification. *IEEE Transactions on Pattern Analysis and Machine Intelligence*, 38(7):1425–1438, 2015. ISSN 0162-8828. doi: 10.1109/tpami.2015.2487986.
- [53] Oriol Vinyals, Charles Blundell, Timothy Lillicrap, Koray Kavukcuoglu, and Daan Wierstra. Matching networks for one shot learning. *arXiv*, 2016. doi: 10.48550/arxiv.1606.04080.
- [54] Xi Yin, Xiang Yu, Kihyuk Sohn, Xiaoming Liu, and Manmohan Chandraker. Feature transfer learning for face recognition with under-represented data. *2019 IEEE/CVF Conference on Computer Vision and Pattern Recognition (CVPR)*, 00:5697–5706, 2019. doi: 10.1109/cvpr.2019.00585.
- [55] Olga Russakovsky, Jia Deng, Hao Su, Jonathan Krause, Sanjeev Satheesh, Sean Ma, Zhiheng Huang, Andrej Karpathy, Aditya Khosla, Michael Bernstein, Alexander C. Berg, and Li Fei-Fei. Imagenet large scale visual recognition challenge. *International Journal of Computer Vision*, 115(3):211–252, 2015. ISSN 0920-5691. doi: 10.1007/s11263-015-0816-y.
- [56] Bolei Zhou, Agata Lapedriza, Aditya Khosla, Aude Oliva, and Antonio Torralba. Places: A 10 million image database for scene recognition. *IEEE Transactions on Pattern Analysis and Machine Intelligence*, 40(6):1452–1464, 2017. ISSN 0162-8828. doi: 10.1109/tpami.2017.2723009.
- [57] Alex Krizhevsky and Geoffrey Hinton. Learning multiple layers of features from tiny images. Technical report, University of Toronto, 2009.
- [58] Grant Van Horn, Oisin Mac Aodha, Yang Song, Yin Cui, Chen Sun, Alex Shepard, Hartwig Adam, Pietro Perona, and Serge Belongie. The inaturalist species classification and detection dataset. *2018 IEEE/CVF Conference on Computer Vision and Pattern Recognition*, pages 8769–8778, 2018. doi: 10.1109/cvpr.2018.00914.
- [59] Joseph Redmon, Santosh Divvala, Ross Girshick, and Ali Farhadi. You only look once: Unified, real-time object detection. In *Proceedings of the IEEE conference on computer vision and pattern recognition*, pages 779–788, 2016.
- [60] Ilya Loshchilov and Frank Hutter. Decoupled weight decay regularization. *arXiv*, 2017. doi: 10.48550/arxiv.1711.05101.

Appendix A Additional Results

This document contains additional analysis, as well as results on the long-tailed recognition (LTR) model^[10]. The included results are

- Per-split accuracy with varying number of nearest numbers computed using Euclidean and cosine distance (Figure A1).
- Distribution of α values across ‘few’ split classes for different number of nearest numbers computed using Euclidean distance (Figure A2).
- Tables of per-split accuracy comparing AlphaNet trained on a range of ρ values:
 - ImageNet-LT (Table A1, A2, A3).
 - Places-LT (Table A4, A5).
 - CIFAR-100-LT (Table A6, A7).
- Change in per-class accuracy for AlphaNet compared to baseline models:
 - ImageNet-LT (Figure A3, A4, A5).
 - Places-LT (Figure A6, A7).
 - CIFAR-100-LT (Figure A8, A9).
- Per-class test accuracy vs. mean distance to 5 nearest neighbors:
 - ImageNet-LT (Figure A10a, A10b, A10c).
 - Places-LT (Figure A11a, A11b).
 - CIFAR-100-LT (Figure A12a, A12b).
- Distribution of α values across ‘few’ split classes:
 - ImageNet-LT (Figure A13a, A13b, A13c).
 - Places-LT (Figure A14a, A14b).
 - CIFAR-100-LT (Figure A15a, A15b).

Experiment	Few	Med.	Many	Overall
Baseline	27.4	46.2	61.8	49.6
AlphaNet ($\rho = 0.1$)	47.6 ^{1.60}	37.1 ^{0.76}	53.8 ^{0.62}	45.0 ^{0.41}
AlphaNet ($\rho = 0.2$)	45.7 ^{1.56}	39.0 ^{0.78}	55.7 ^{0.79}	46.3 ^{0.52}
AlphaNet ($\rho = 0.25$)	44.1 ^{1.44}	40.2 ^{0.65}	56.7 ^{0.57}	47.1 ^{0.36}
AlphaNet ($\rho = 0.3$)	42.9 ^{1.29}	40.4 ^{0.72}	57.0 ^{0.68}	47.1 ^{0.47}
AlphaNet ($\rho = 0.4$)	40.8 ^{1.85}	41.5 ^{0.72}	57.8 ^{0.54}	47.7 ^{0.36}
AlphaNet ($\rho = 0.5$)	39.7 ^{1.42}	42.0 ^{0.66}	58.3 ^{0.52}	48.0 ^{0.37}
AlphaNet ($\rho = 0.75$)	37.4 ^{1.93}	42.9 ^{0.46}	59.0 ^{0.40}	48.3 ^{0.16}
AlphaNet ($\rho = 1$)	34.6 ^{1.88}	43.7 ^{0.51}	59.7 ^{0.43}	48.6 ^{0.24}
AlphaNet ($\rho = 1.25$)	35.0 ^{1.98}	43.6 ^{0.70}	59.6 ^{0.50}	48.6 ^{0.35}
AlphaNet ($\rho = 1.5$)	32.6 ^{2.46}	44.4 ^{0.49}	60.3 ^{0.38}	48.9 ^{0.19}
AlphaNet ($\rho = 1.75$)	32.3 ^{1.42}	44.4 ^{0.32}	60.3 ^{0.18}	48.9 ^{0.14}
AlphaNet ($\rho = 2$)	31.5 ^{1.99}	44.7 ^{0.46}	60.5 ^{0.30}	49.0 ^{0.12}
AlphaNet ($\rho = 3$)	29.0 ^{2.05}	45.1 ^{0.36}	60.9 ^{0.28}	49.0 ^{0.08}

Table A1: AlphaNet with CRT baseline on ImageNet-LT.

Experiment	Few	Med.	Many	Overall
Baseline	30.4	47.2	60.2	49.9
AlphaNet ($\rho = 0.1$)	53.9 ^{0.77}	29.4 ^{1.22}	44.2 ^{1.22}	38.5 ^{1.03}
AlphaNet ($\rho = 0.2$)	52.0 ^{1.21}	33.3 ^{1.44}	48.0 ^{1.37}	41.5 ^{1.08}
AlphaNet ($\rho = 0.25$)	51.1 ^{0.63}	34.4 ^{1.04}	48.9 ^{0.99}	42.3 ^{0.82}
AlphaNet ($\rho = 0.3$)	49.8 ^{2.20}	35.9 ^{1.59}	50.4 ^{1.47}	43.4 ^{1.10}
AlphaNet ($\rho = 0.4$)	48.7 ^{1.17}	37.4 ^{1.13}	51.6 ^{0.95}	44.4 ^{0.80}
AlphaNet ($\rho = 0.5$)	46.9 ^{0.98}	38.6 ^{0.87}	52.9 ^{0.86}	45.3 ^{0.69}
AlphaNet ($\rho = 0.75$)	45.3 ^{1.89}	40.2 ^{1.28}	54.4 ^{1.01}	46.3 ^{0.76}
AlphaNet ($\rho = 1$)	41.6 ^{1.61}	42.2 ^{0.53}	56.0 ^{0.32}	47.4 ^{0.30}
AlphaNet ($\rho = 1.25$)	42.5 ^{1.41}	42.1 ^{0.74}	56.0 ^{0.53}	47.5 ^{0.41}
AlphaNet ($\rho = 1.5$)	40.1 ^{1.99}	43.2 ^{0.98}	56.9 ^{0.76}	48.0 ^{0.53}
AlphaNet ($\rho = 1.75$)	39.4 ^{2.53}	43.5 ^{0.88}	57.1 ^{0.70}	48.2 ^{0.45}
AlphaNet ($\rho = 2$)	37.5 ^{2.94}	44.3 ^{0.86}	57.9 ^{0.72}	48.6 ^{0.32}
AlphaNet ($\rho = 3$)	34.5 ^{1.91}	45.3 ^{0.54}	58.7 ^{0.37}	49.0 ^{0.21}

Table A2: AlphaNet with LWS baseline on ImageNet-LT.

Experiment	Few	Med.	Many	Overall
Baseline	36.5	54.4	68.9	57.5
AlphaNet ($\rho = 0.1$)	49.2 ^{0.69}	49.5 ^{0.40}	65.4 ^{0.16}	55.6 ^{0.19}
AlphaNet ($\rho = 0.2$)	47.1 ^{0.86}	50.5 ^{0.34}	66.0 ^{0.20}	56.0 ^{0.16}
AlphaNet ($\rho = 0.25$)	46.8 ^{0.59}	50.7 ^{0.29}	66.2 ^{0.25}	56.2 ^{0.23}
AlphaNet ($\rho = 0.3$)	46.1 ^{1.16}	51.2 ^{0.50}	66.5 ^{0.29}	56.4 ^{0.21}
AlphaNet ($\rho = 0.4$)	44.7 ^{1.13}	51.7 ^{0.39}	66.9 ^{0.24}	56.6 ^{0.22}
AlphaNet ($\rho = 0.5$)	43.5 ^{0.75}	52.3 ^{0.26}	67.3 ^{0.17}	56.9 ^{0.11}
AlphaNet ($\rho = 0.75$)	41.7 ^{0.63}	52.8 ^{0.18}	67.7 ^{0.15}	57.0 ^{0.12}
AlphaNet ($\rho = 1$)	40.8 ^{1.00}	53.1 ^{0.21}	67.9 ^{0.18}	57.1 ^{0.11}
AlphaNet ($\rho = 1.25$)	39.0 ^{1.28}	53.4 ^{0.22}	68.2 ^{0.16}	57.2 ^{0.05}
AlphaNet ($\rho = 1.5$)	38.2 ^{1.22}	53.6 ^{0.25}	68.4 ^{0.17}	57.2 ^{0.06}
AlphaNet ($\rho = 1.75$)	37.7 ^{0.89}	53.7 ^{0.14}	68.4 ^{0.10}	57.2 ^{0.05}
AlphaNet ($\rho = 2$)	37.1 ^{0.98}	53.8 ^{0.12}	68.5 ^{0.11}	57.2 ^{0.06}
AlphaNet ($\rho = 3$)	34.5 ^{1.23}	54.3 ^{0.14}	68.8 ^{0.11}	57.2 ^{0.08}

Table A3: AlphaNet with RIDE baseline on ImageNet-LT.

Experiment	Few	Med.	Many	Overall
Baseline	24.9	37.6	42.0	36.7
AlphaNet ($\rho = 0.1$)	38.21 ^{.30}	30.49 ^{.84}	37.39 ^{.72}	34.40 ^{.41}
AlphaNet ($\rho = 0.2$)	34.81 ^{.42}	32.49 ^{.66}	39.09 ^{.29}	35.30 ^{.15}
AlphaNet ($\rho = 0.25$)	34.41 ^{.27}	32.80 ^{.82}	39.30 ^{.34}	35.50 ^{.29}
AlphaNet ($\rho = 0.3$)	33.21 ^{.57}	33.49 ^{.75}	39.50 ^{.60}	35.60 ^{.25}
AlphaNet ($\rho = 0.4$)	32.41 ^{.47}	33.80 ^{.69}	39.80 ^{.46}	35.70 ^{.22}
AlphaNet ($\rho = 0.5$)	31.09 ^{.88}	34.50 ^{.17}	40.40 ^{.29}	35.90 ^{.09}
AlphaNet ($\rho = 0.75$)	28.61 ^{.27}	35.59 ^{.40}	41.09 ^{.13}	36.10 ^{.11}
AlphaNet ($\rho = 1$)	27.01 ^{.02}	36.10 ^{.31}	41.30 ^{.13}	36.20 ^{.10}
AlphaNet ($\rho = 1.25$)	26.91 ^{.23}	36.00 ^{.47}	41.30 ^{.14}	36.10 ^{.16}
AlphaNet ($\rho = 1.5$)	25.59 ^{.89}	36.50 ^{.36}	41.60 ^{.21}	36.20 ^{.11}
AlphaNet ($\rho = 1.75$)	25.41 ^{.32}	36.50 ^{.29}	41.50 ^{.23}	36.20 ^{.11}
AlphaNet ($\rho = 2$)	24.91 ^{.38}	36.60 ^{.49}	41.50 ^{.20}	36.10 ^{.10}
AlphaNet ($\rho = 3$)	22.31 ^{.56}	37.30 ^{.28}	41.90 ^{.20}	36.10 ^{.14}

Table A4: AlphaNet with cRT baseline on Places-LT.

Experiment	Few	Med.	Many	Overall
Baseline	33.6	49.4	69.7	51.8
AlphaNet ($\rho = 0.1$)	40.94 ^{.12}	37.47 ^{.63}	62.15 ^{.07}	47.13 ^{.27}
AlphaNet ($\rho = 0.2$)	42.62 ^{.47}	32.94 ^{.98}	58.73 ^{.36}	44.82 ^{.43}
AlphaNet ($\rho = 0.25$)	42.32 ^{.45}	34.46 ^{.36}	59.54 ^{.83}	45.53 ^{.31}
AlphaNet ($\rho = 0.3$)	40.93 ^{.77}	36.66 ^{.76}	61.34 ^{.78}	46.63 ^{.14}
AlphaNet ($\rho = 0.4$)	42.31 ^{.73}	33.16 ^{.20}	58.94 ^{.24}	44.93 ^{.25}
AlphaNet ($\rho = 0.5$)	43.21 ^{.17}	32.14 ^{.73}	58.73 ^{.55}	44.72 ^{.64}
AlphaNet ($\rho = 0.75$)	43.11 ^{.45}	31.35 ^{.14}	57.74 ^{.01}	44.12 ^{.95}
AlphaNet ($\rho = 1$)	42.52 ^{.31}	31.36 ^{.45}	57.44 ^{.50}	43.83 ^{.21}
AlphaNet ($\rho = 1.25$)	41.74 ^{.03}	33.48 ^{.11}	59.15 ^{.61}	44.93 ^{.91}
AlphaNet ($\rho = 1.5$)	43.69 ^{.87}	31.33 ^{.49}	57.82 ^{.57}	44.31 ^{.95}
AlphaNet ($\rho = 1.75$)	42.70 ^{.70}	30.04 ^{.75}	56.53 ^{.51}	43.12 ^{.93}
AlphaNet ($\rho = 2$)	43.10 ^{.79}	28.41 ^{.86}	55.41 ^{.59}	42.21 ^{.39}
AlphaNet ($\rho = 3$)	43.20 ^{.93}	28.02 ^{.00}	55.31 ^{.45}	42.11 ^{.43}

Table A7: AlphaNet with LTR baseline on CIFAR-100-LT.

Experiment	Few	Med.	Many	Overall
Baseline	28.7	39.1	40.6	37.6
AlphaNet ($\rho = 0.1$)	42.51 ^{.03}	29.51 ^{.01}	34.40 ^{.94}	33.80 ^{.58}
AlphaNet ($\rho = 0.2$)	41.31 ^{.30}	31.09 ^{.81}	35.50 ^{.81}	34.60 ^{.44}
AlphaNet ($\rho = 0.25$)	40.52 ^{.25}	30.92 ^{.92}	35.62 ^{.20}	34.41 ^{.67}
AlphaNet ($\rho = 0.3$)	38.71 ^{.13}	33.21 ^{.12}	37.00 ^{.70}	35.60 ^{.51}
AlphaNet ($\rho = 0.4$)	38.01 ^{.45}	33.61 ^{.18}	37.30 ^{.65}	35.80 ^{.50}
AlphaNet ($\rho = 0.5$)	37.11 ^{.39}	34.40 ^{.80}	37.70 ^{.52}	36.10 ^{.31}
AlphaNet ($\rho = 0.75$)	35.51 ^{.25}	35.30 ^{.59}	38.50 ^{.28}	36.50 ^{.16}
AlphaNet ($\rho = 1$)	34.69 ^{.97}	35.80 ^{.54}	38.60 ^{.39}	36.60 ^{.22}
AlphaNet ($\rho = 1.25$)	32.61 ^{.28}	36.80 ^{.60}	39.30 ^{.39}	36.90 ^{.19}
AlphaNet ($\rho = 1.5$)	32.21 ^{.17}	37.29 ^{.36}	39.50 ^{.39}	37.00 ^{.11}
AlphaNet ($\rho = 1.75$)	31.71 ^{.35}	37.30 ^{.43}	39.50 ^{.27}	37.00 ^{.09}
AlphaNet ($\rho = 2$)	30.91 ^{.28}	37.60 ^{.40}	39.80 ^{.18}	37.10 ^{.14}
AlphaNet ($\rho = 3$)	27.81 ^{.94}	38.50 ^{.51}	40.20 ^{.29}	37.10 ^{.10}

Table A5: AlphaNet with LWS baseline on Places-LT.

Experiment	Few	Med.	Many	Overall
Baseline	25.8	52.1	69.3	50.2
AlphaNet ($\rho = 0.1$)	38.23 ^{.22}	38.15 ^{.01}	56.37 ^{.65}	44.53 ^{.50}
AlphaNet ($\rho = 0.2$)	36.04 ^{.34}	41.45 ^{.41}	59.18 ^{.31}	45.93 ^{.58}
AlphaNet ($\rho = 0.25$)	34.01 ^{.70}	44.11 ^{.68}	62.61 ^{.54}	47.60 ^{.76}
AlphaNet ($\rho = 0.3$)	32.91 ^{.20}	45.31 ^{.02}	64.00 ^{.78}	48.10 ^{.51}
AlphaNet ($\rho = 0.4$)	31.11 ^{.27}	45.61 ^{.63}	64.81 ^{.22}	48.00 ^{.84}
AlphaNet ($\rho = 0.5$)	30.91 ^{.82}	47.01 ^{.25}	65.70 ^{.94}	48.70 ^{.41}
AlphaNet ($\rho = 0.75$)	28.61 ^{.63}	48.30 ^{.84}	66.60 ^{.65}	48.80 ^{.26}
AlphaNet ($\rho = 1$)	27.21 ^{.69}	49.10 ^{.85}	67.49 ^{.62}	48.90 ^{.30}
AlphaNet ($\rho = 1.25$)	26.11 ^{.54}	49.80 ^{.59}	68.00 ^{.47}	49.10 ^{.42}
AlphaNet ($\rho = 1.5$)	25.01 ^{.15}	50.11 ^{.12}	67.91 ^{.01}	48.80 ^{.63}
AlphaNet ($\rho = 1.75$)	24.81 ^{.09}	50.30 ^{.61}	68.40 ^{.33}	49.00 ^{.27}
AlphaNet ($\rho = 2$)	24.31 ^{.74}	51.09 ^{.55}	68.90 ^{.47}	49.20 ^{.34}
AlphaNet ($\rho = 3$)	22.21 ^{.71}	51.60 ^{.86}	69.30 ^{.58}	49.00 ^{.31}

Table A6: AlphaNet with RIDE baseline on CIFAR-100-LT.

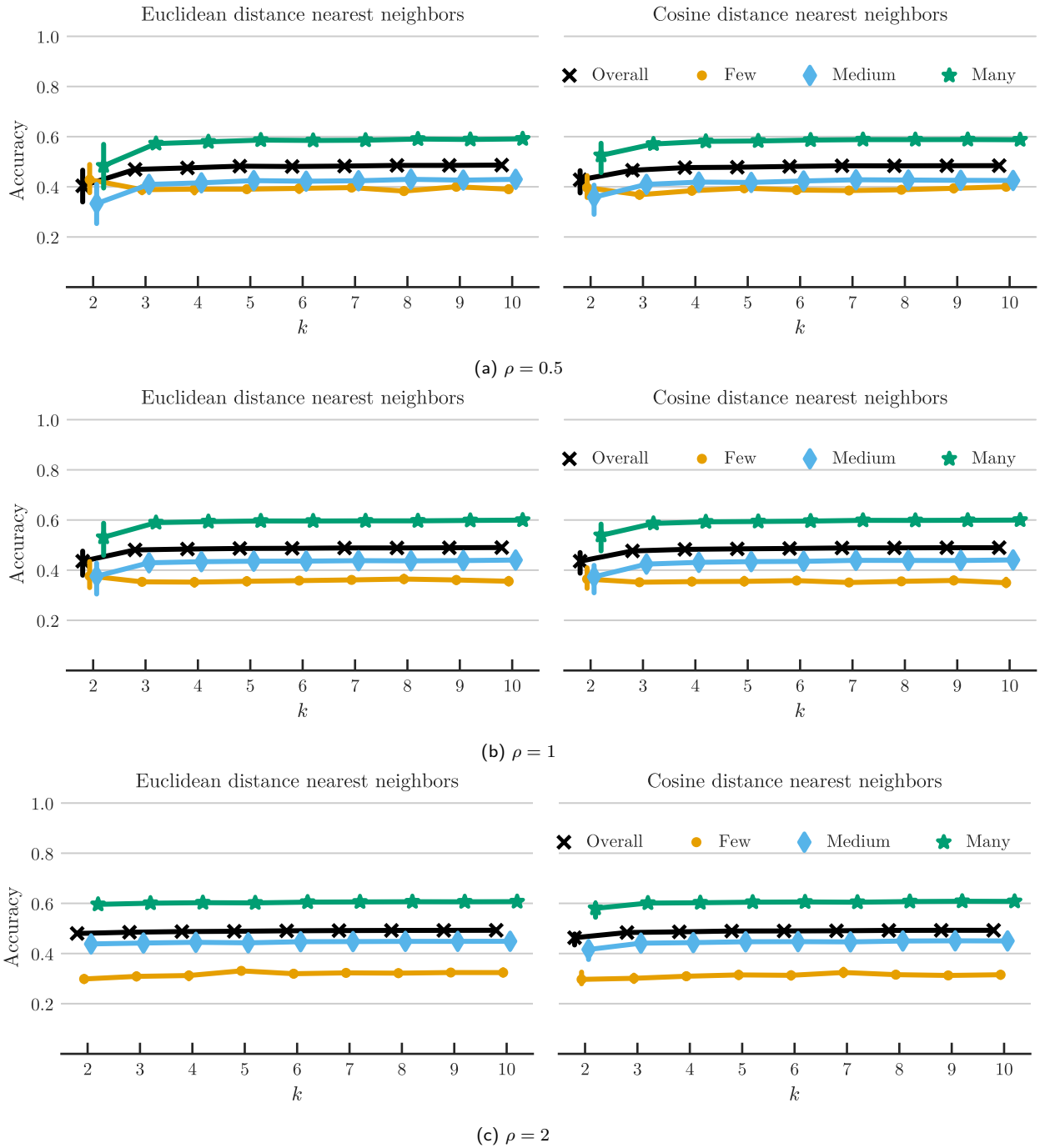


Figure A1: Per-split accuracies on ImageNet-LT with varying number of nearest neighbors for AlphaNet on cRT baseline.

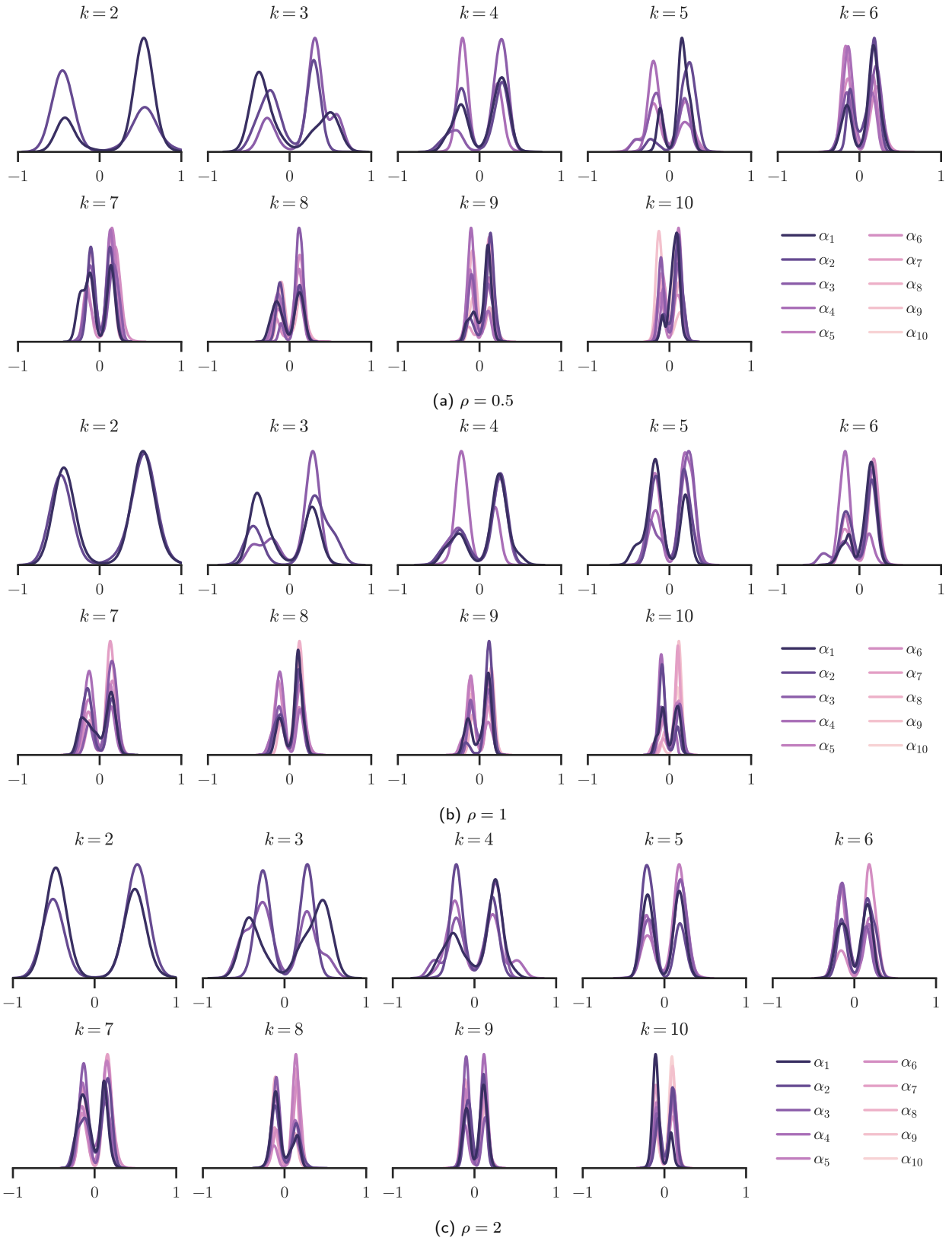


Figure A2: Distribution of α values across k for AlphaNet with cRT baseline trained on ImageNet-LT.

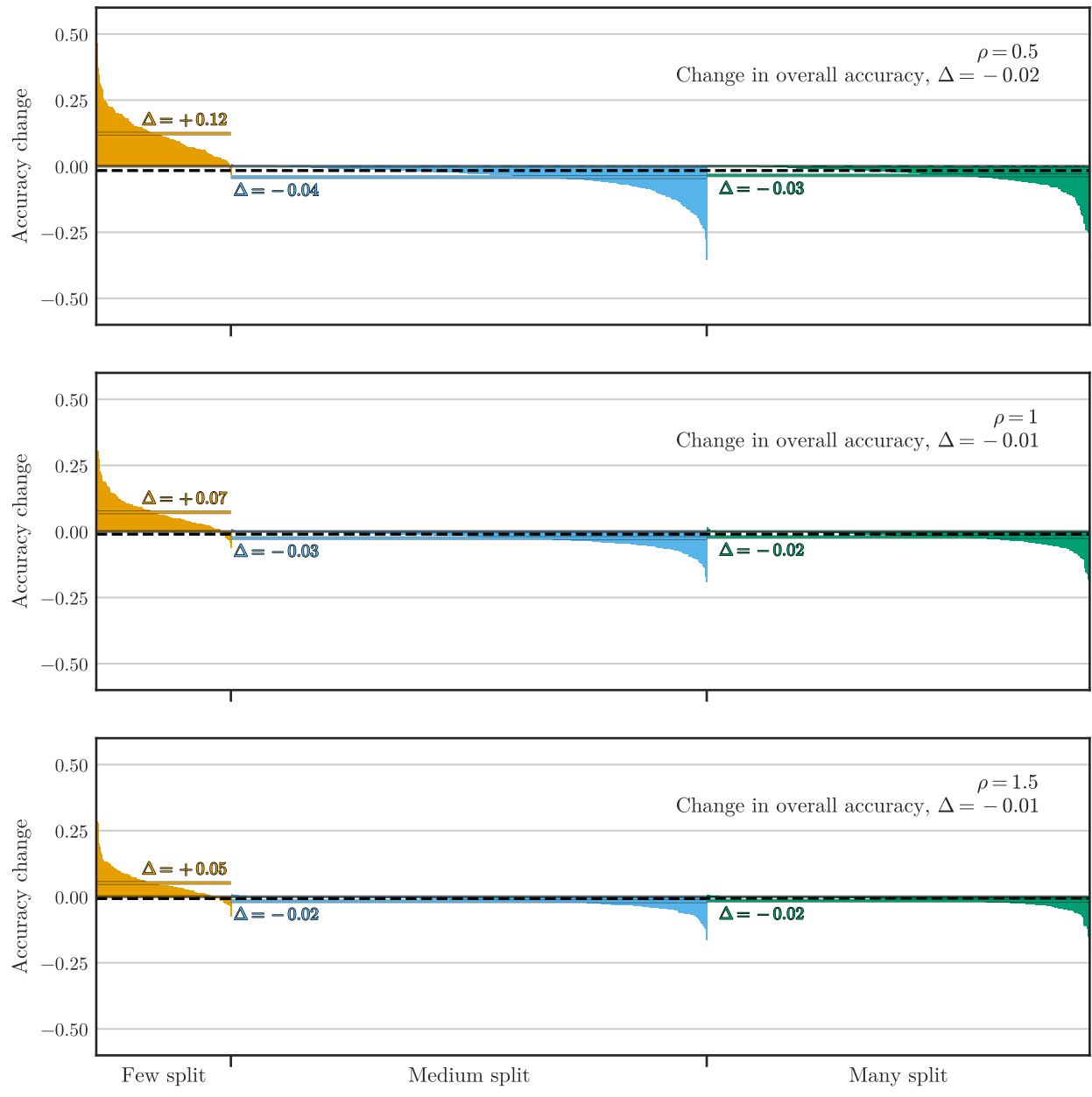


Figure A3: Change in per-class accuracy on ImageNet-LT with AlphaNet on cRT. The Δ s indicate the average change in split accuracy.

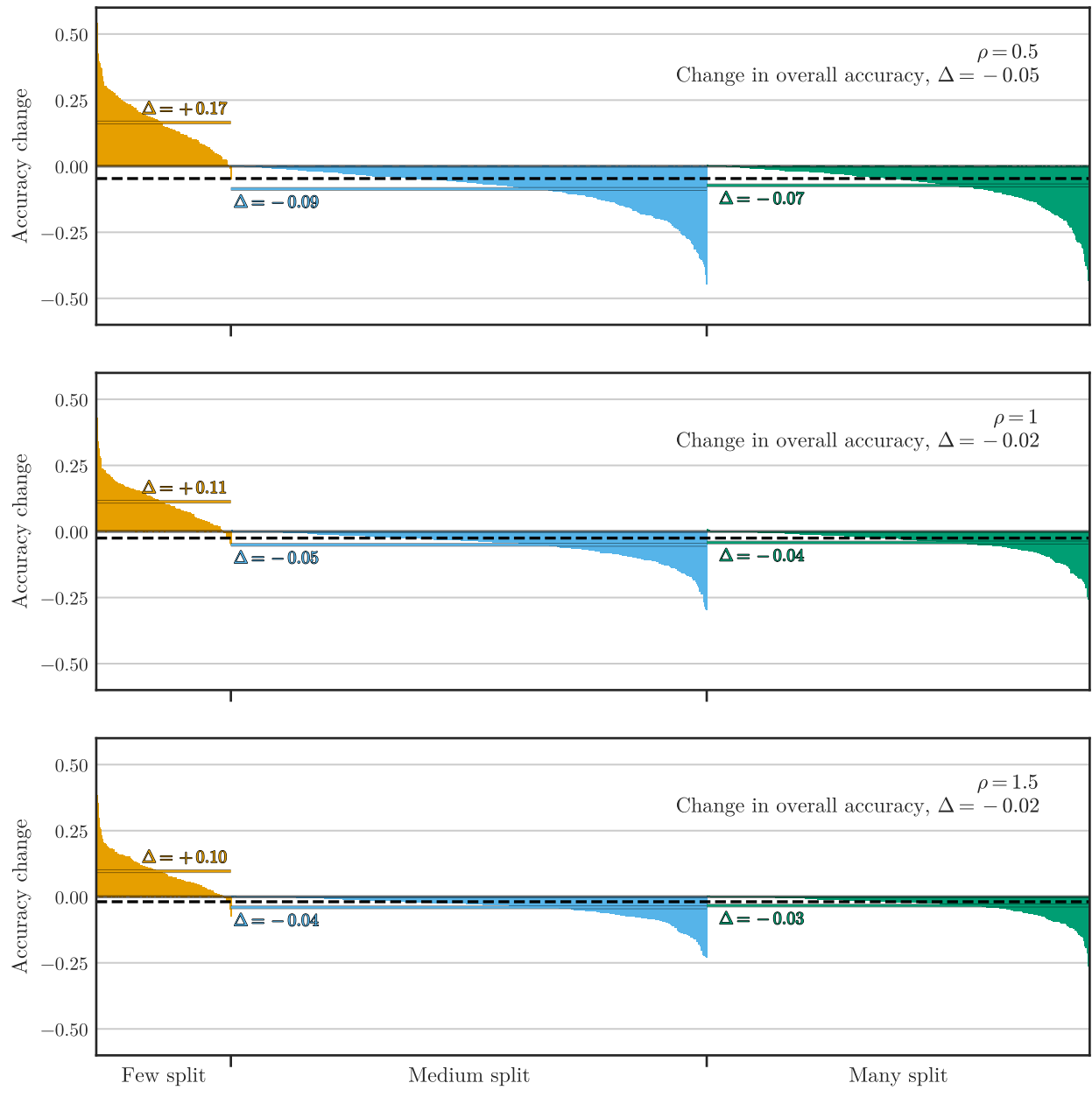


Figure A4: Change in per-class accuracy on ImageNet-LT with AlphaNet on LWS. The Δ s indicate the average change in split accuracy.

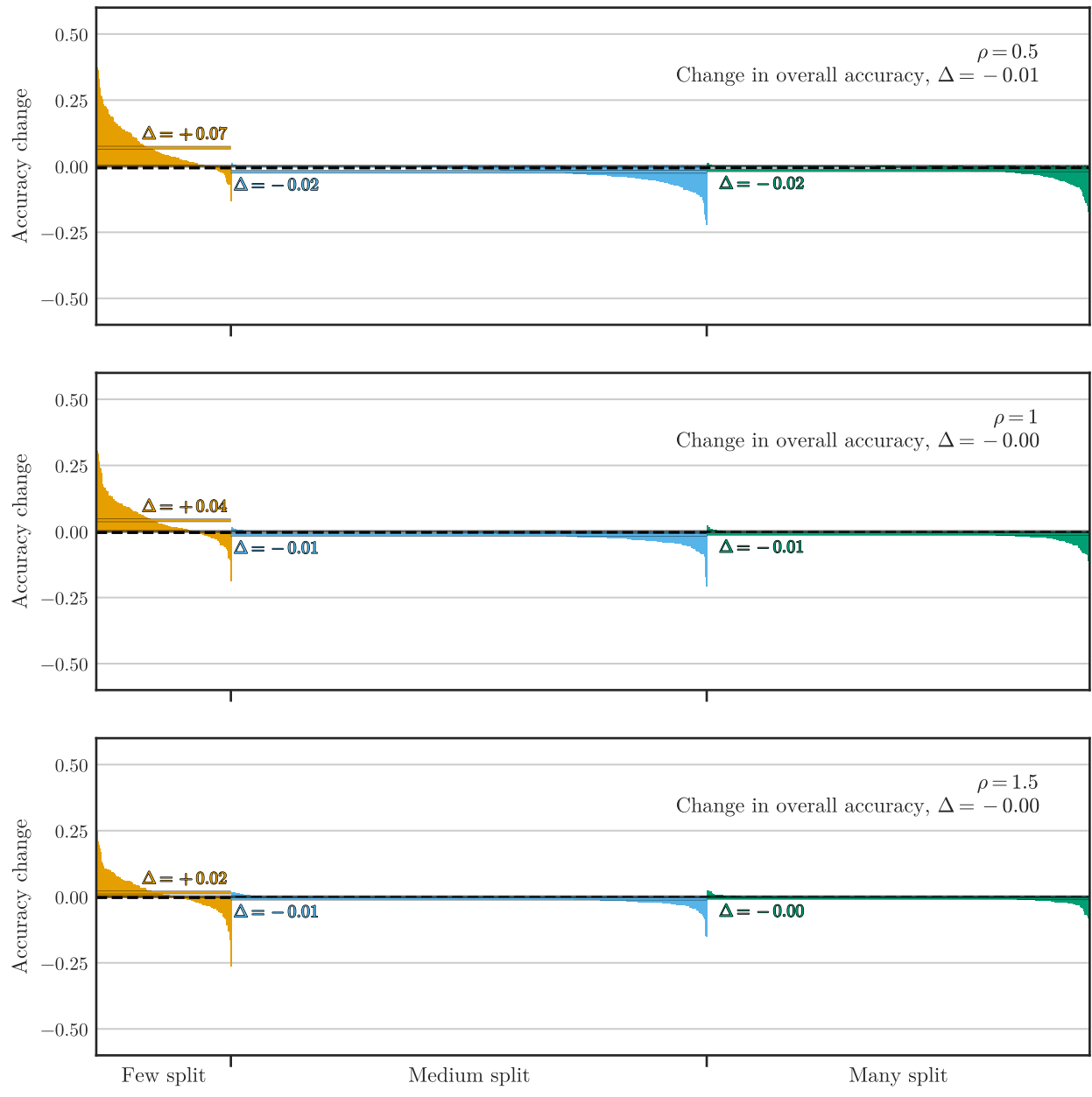


Figure A5: Change in per-class accuracy on ImageNet-LT with AlphaNet on RIDE. The Δ s indicate the average change in split accuracy.

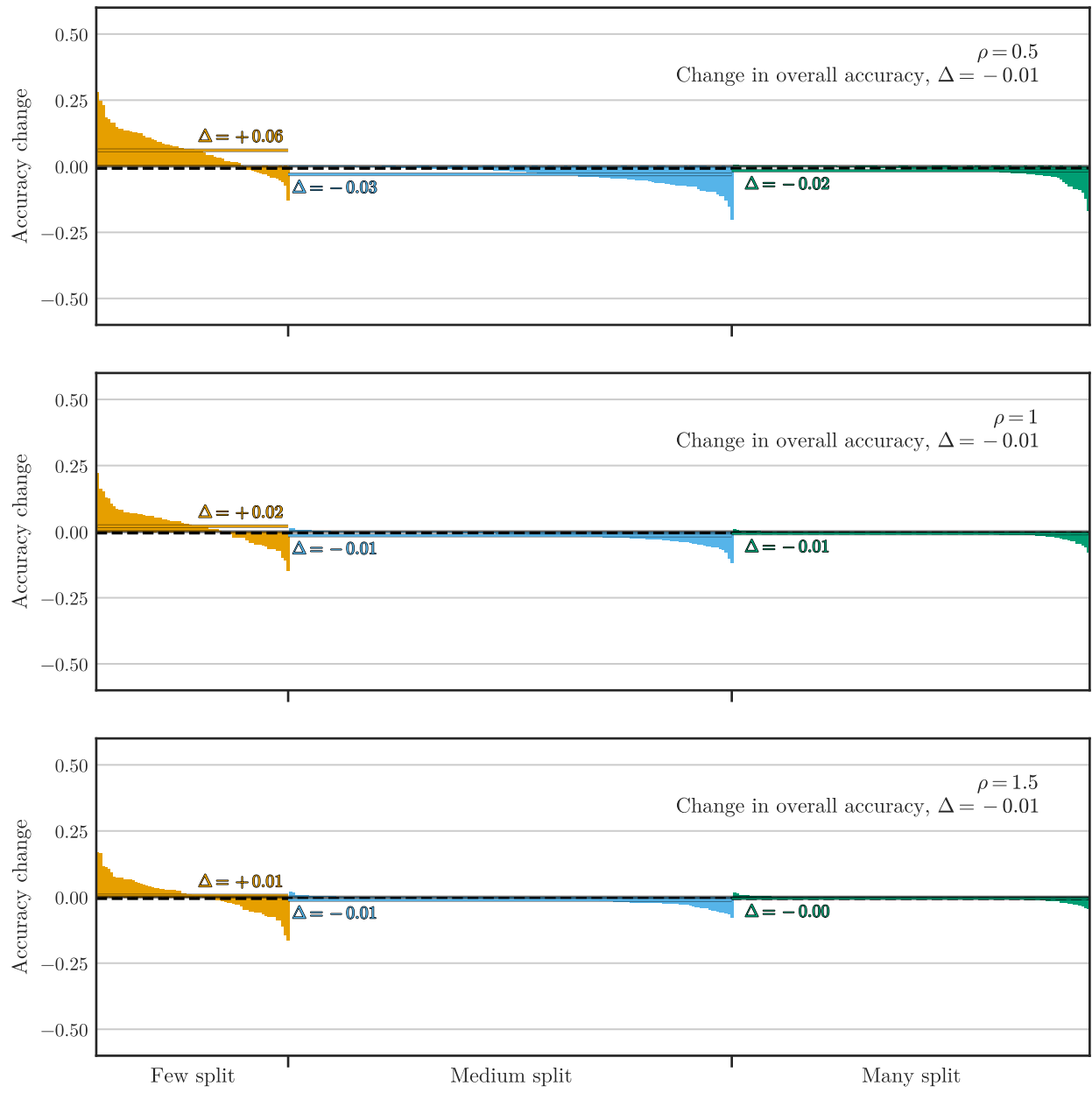


Figure A6: Change in per-class accuracy on Places-LT with AlphaNet on cRT. The Δ s indicate the average change in split accuracy.

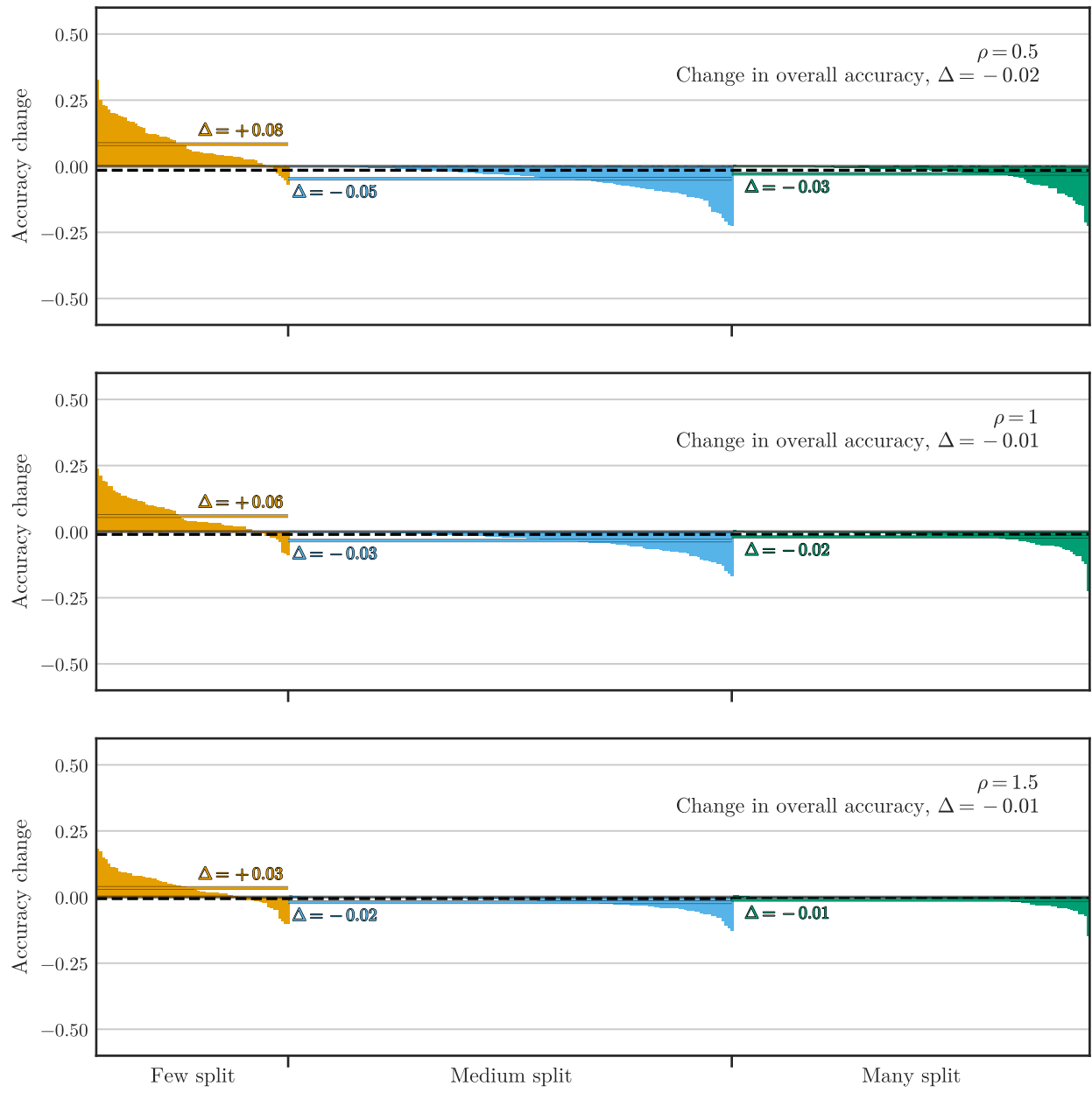


Figure A7: Change in per-class accuracy on Places-LT with AlphaNet on LWS. The Δ s indicate the average change in split accuracy.

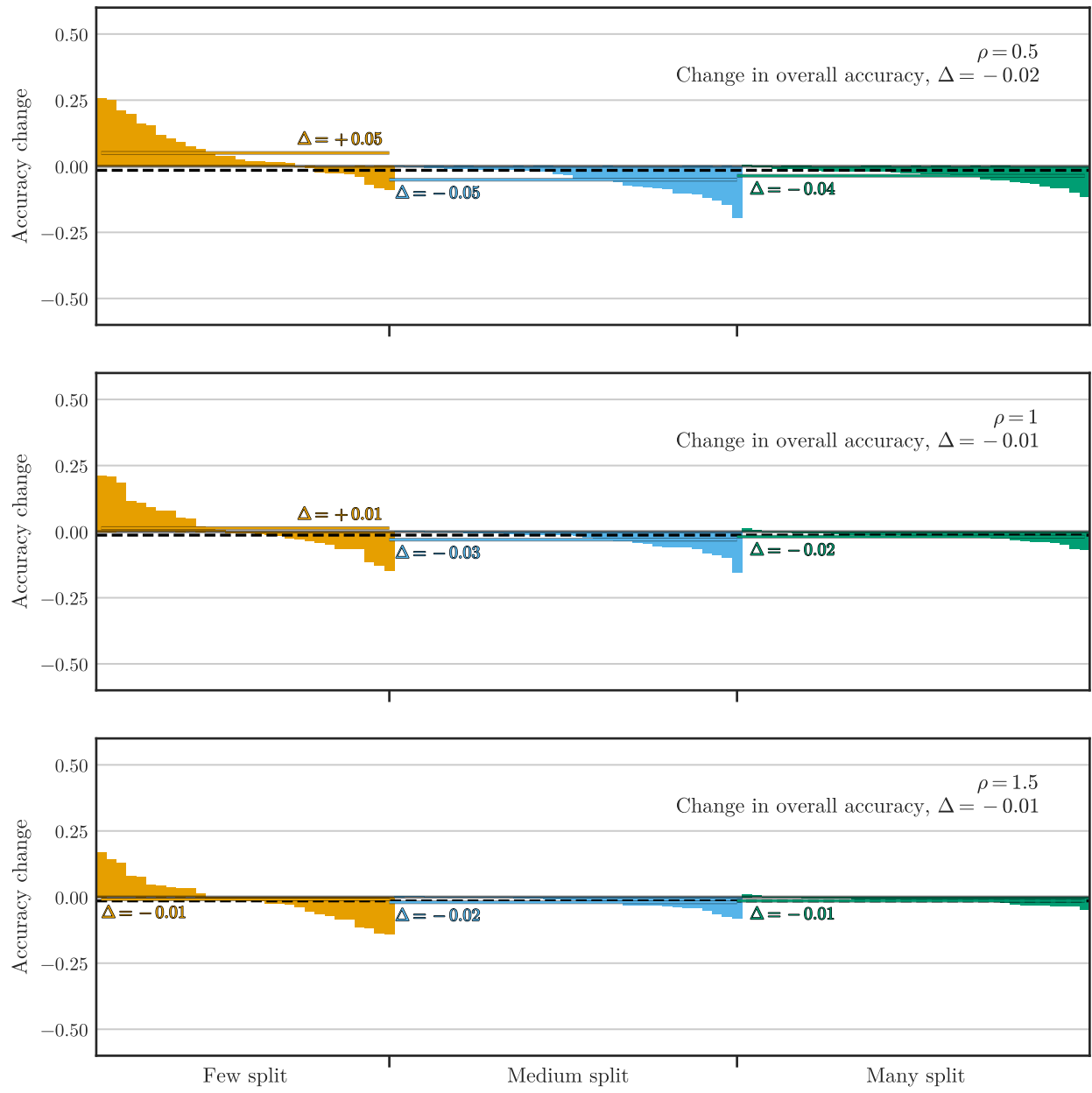


Figure A8: Change in per-class accuracy on CIFAR-100-LT with AlphaNet on RIDE. The Δ s indicate the average change in split accuracy.

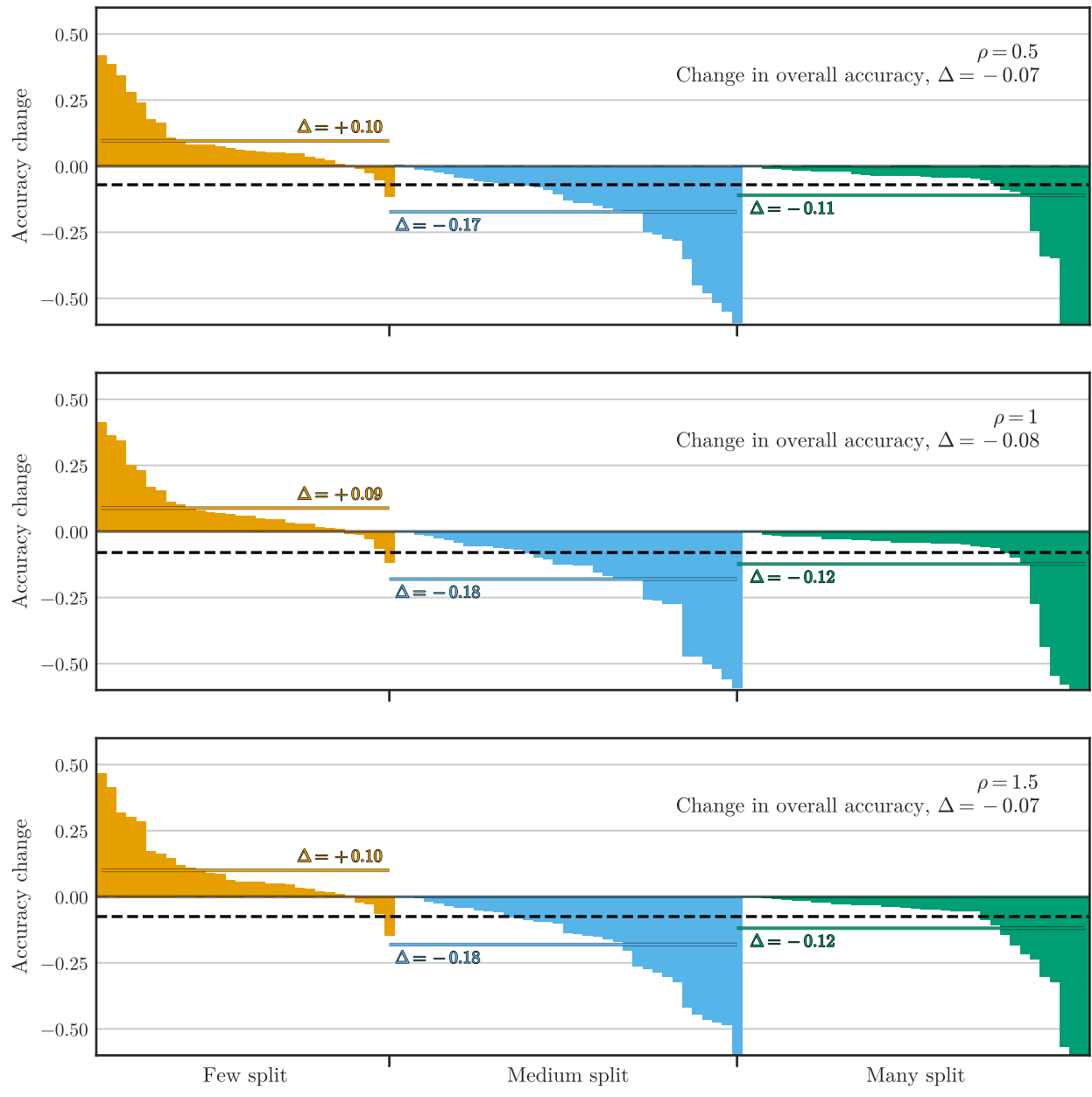


Figure A9: Change in per-class accuracy on CIFAR-100-LT with AlphaNet on LTR. The Δ s indicate the average change in split accuracy.

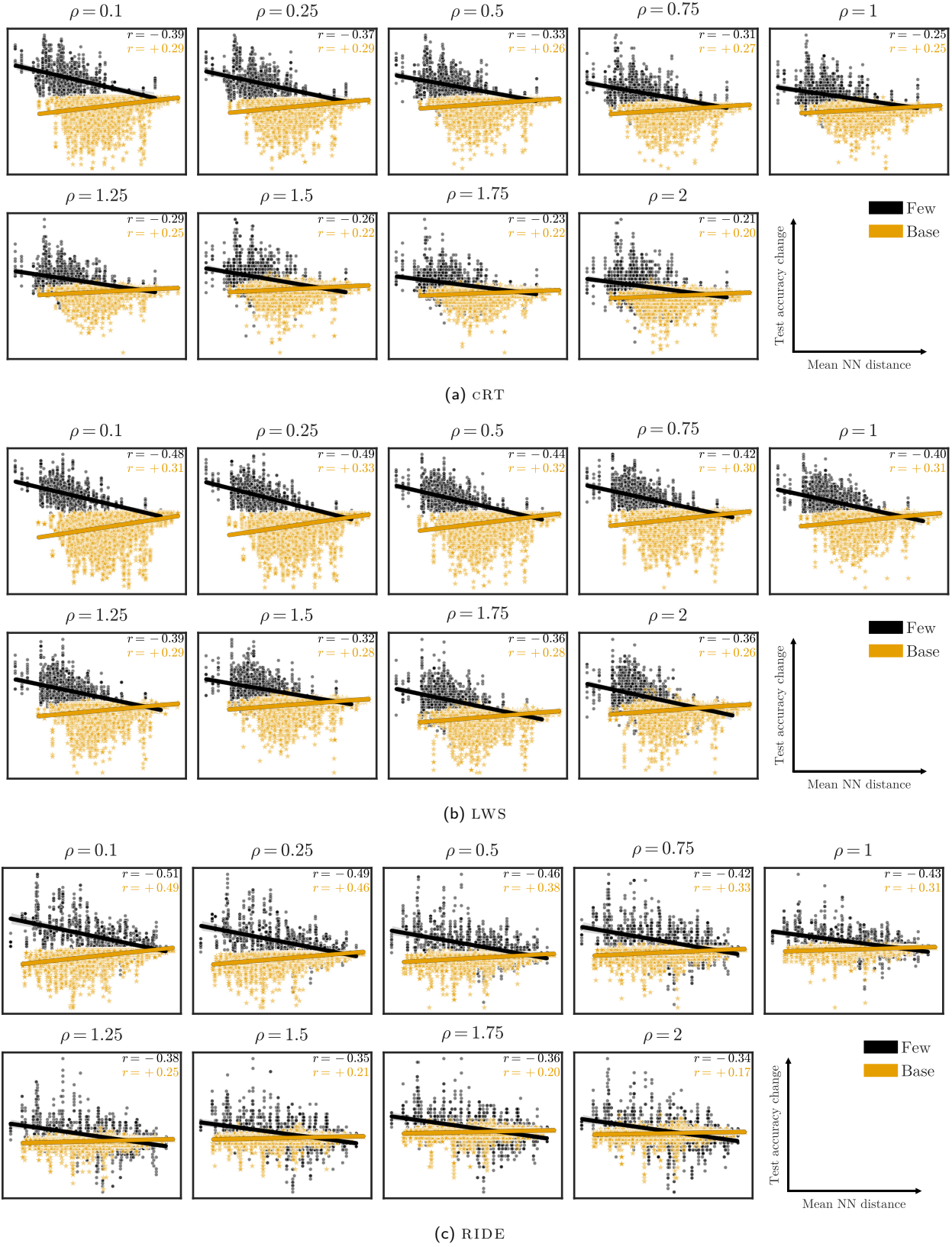


Figure A10: Test accuracy on ImageNet-LT vs. mean nearest neighbor distance for AlphaNet trained with $k = 5$ neighbors. The lines show regression fits, and the r values in the upper right are Pearson correlations.

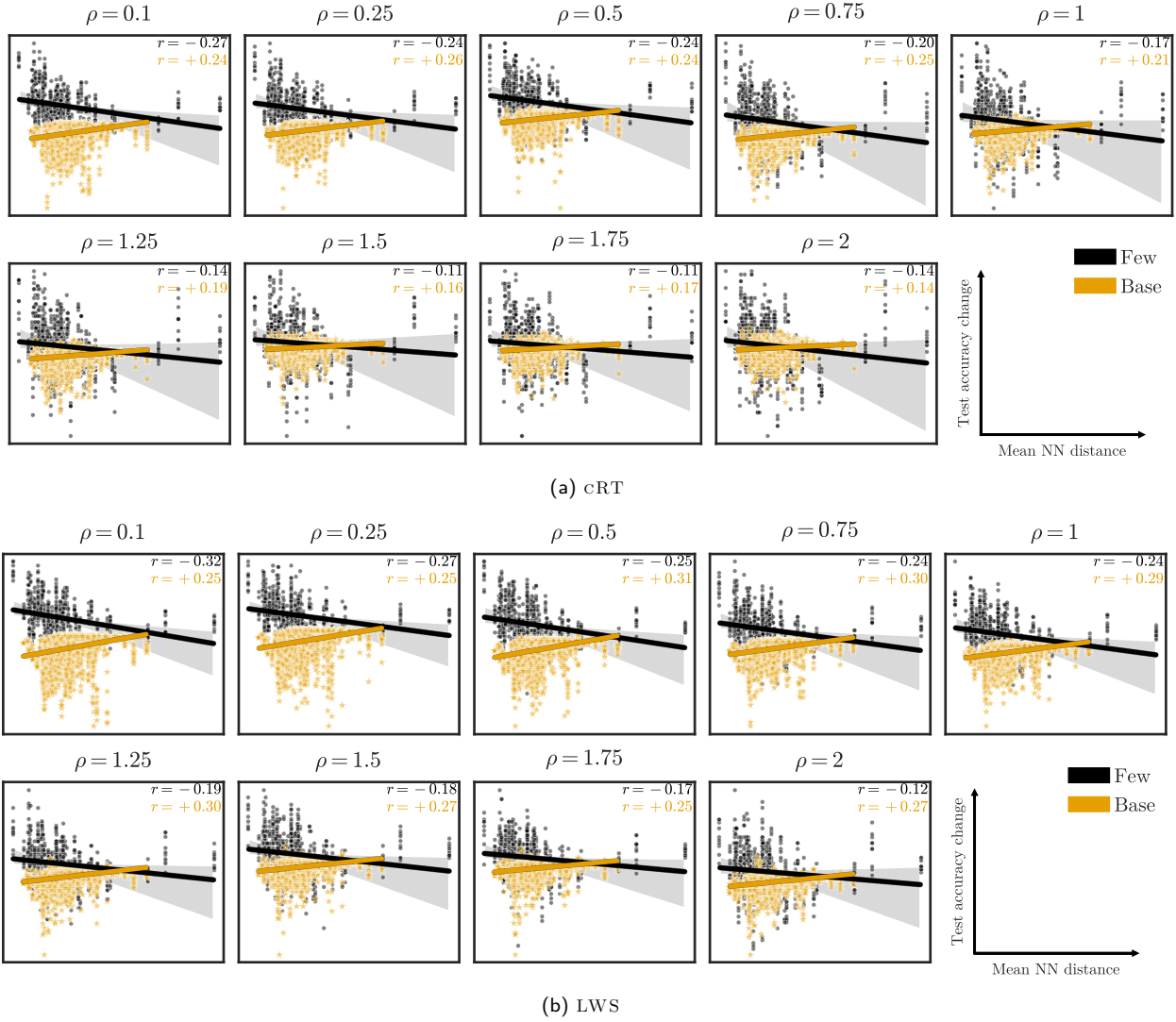


Figure A11: Test accuracy on Places-LT vs. mean nearest neighbor distance for AlphaNet trained with $k = 5$ neighbors. The lines show regression fits, and the r values in the upper right are Pearson correlations.

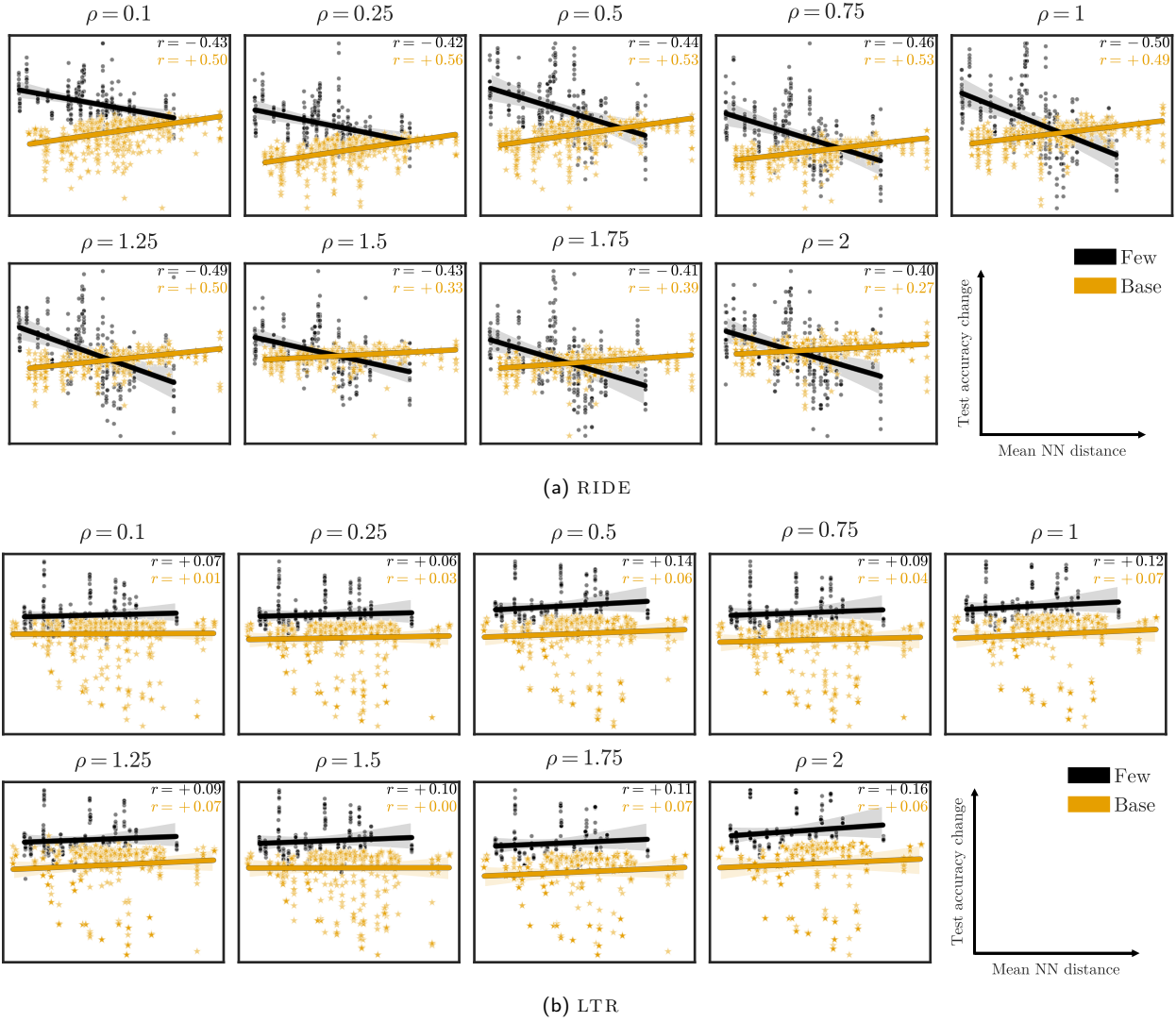


Figure A12: Test accuracy on CIFAR-100-LT vs. mean nearest neighbor distance for AlphaNet trained with $k = 5$ neighbors. The lines show regression fits, and the r values in the upper right are Pearson correlations.

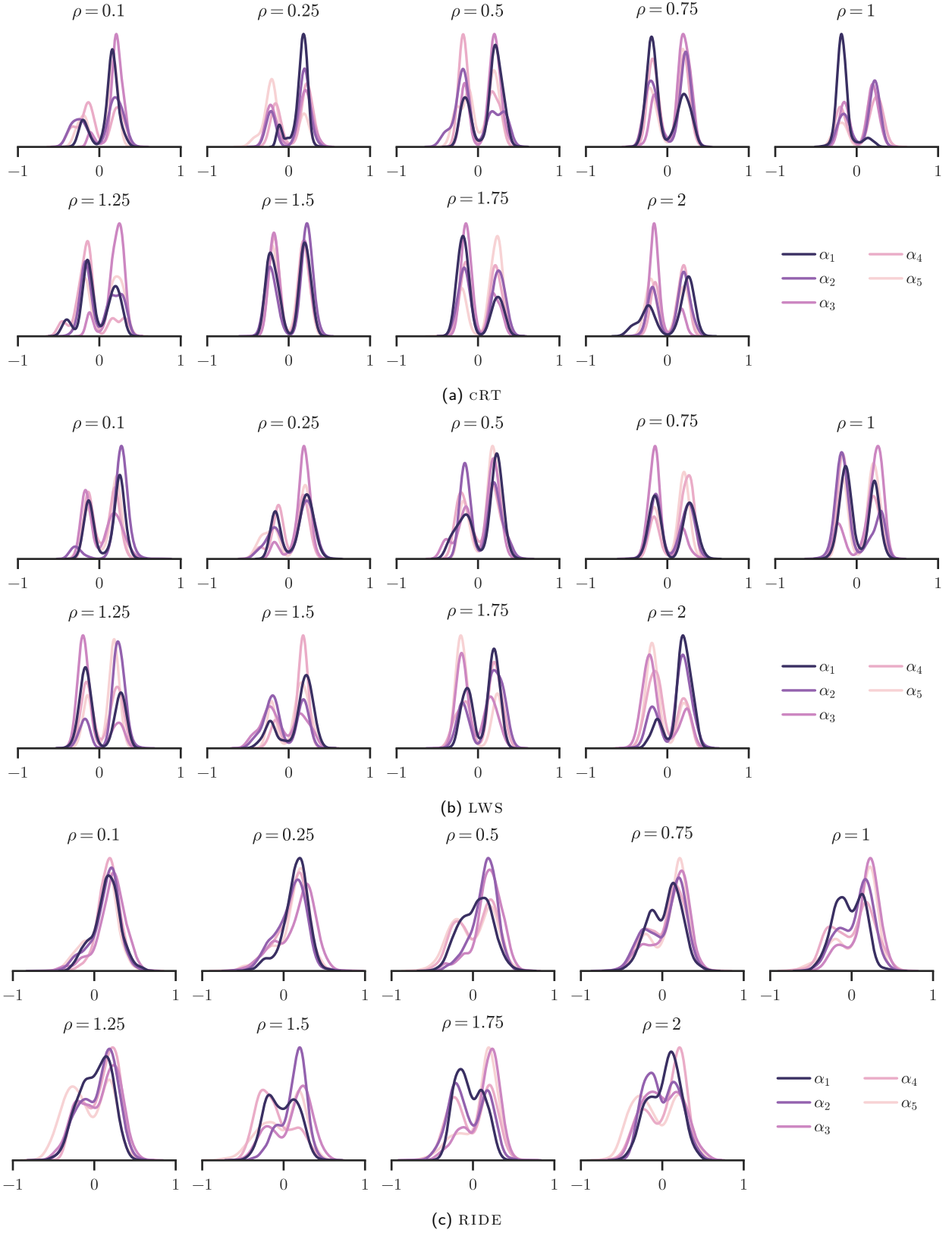


Figure A13: Distribution of α s for AlphaNet trained on ImageNet-LT.

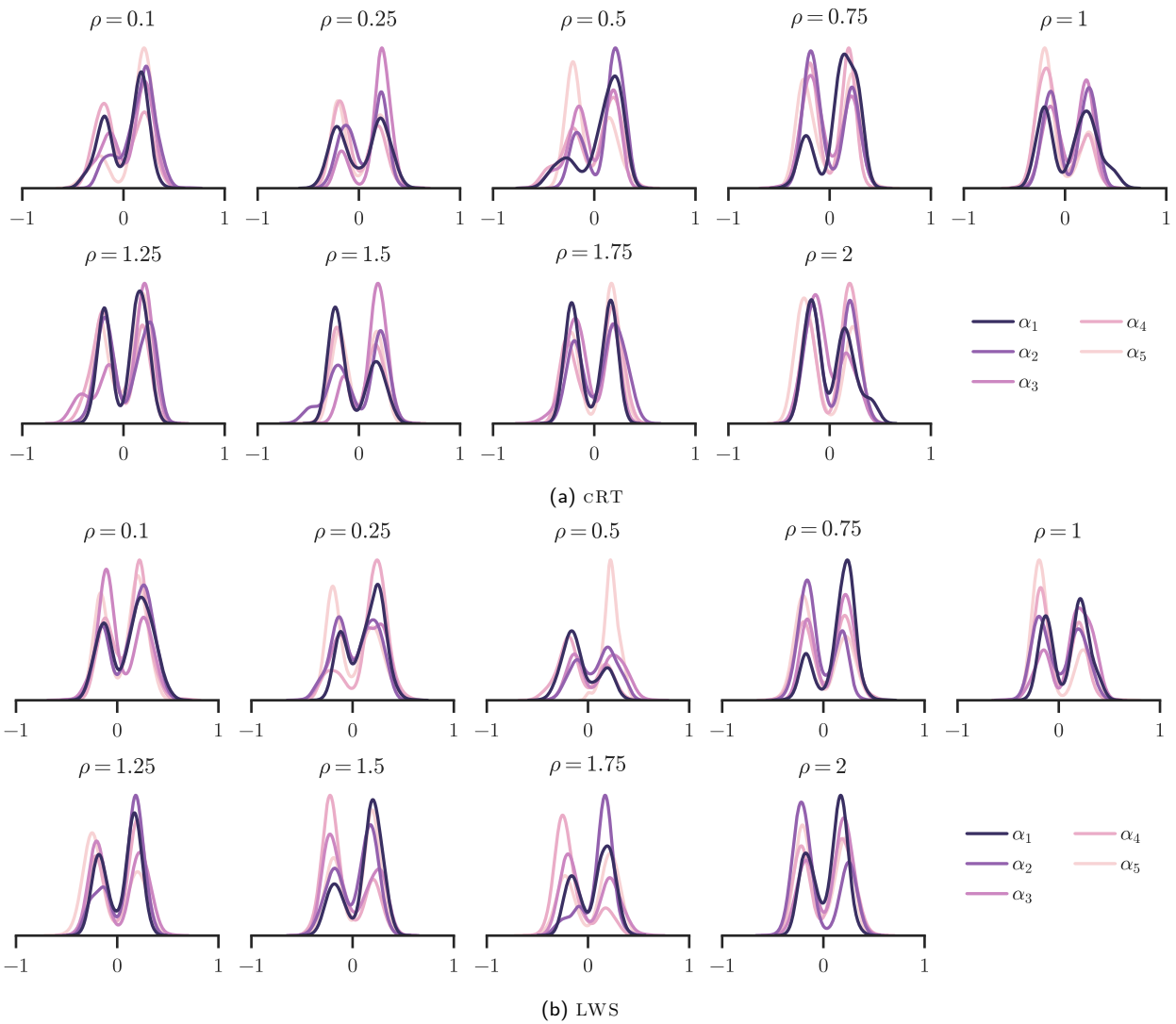


Figure A14: Distribution of α s for AlphaNet trained on Places-LT.

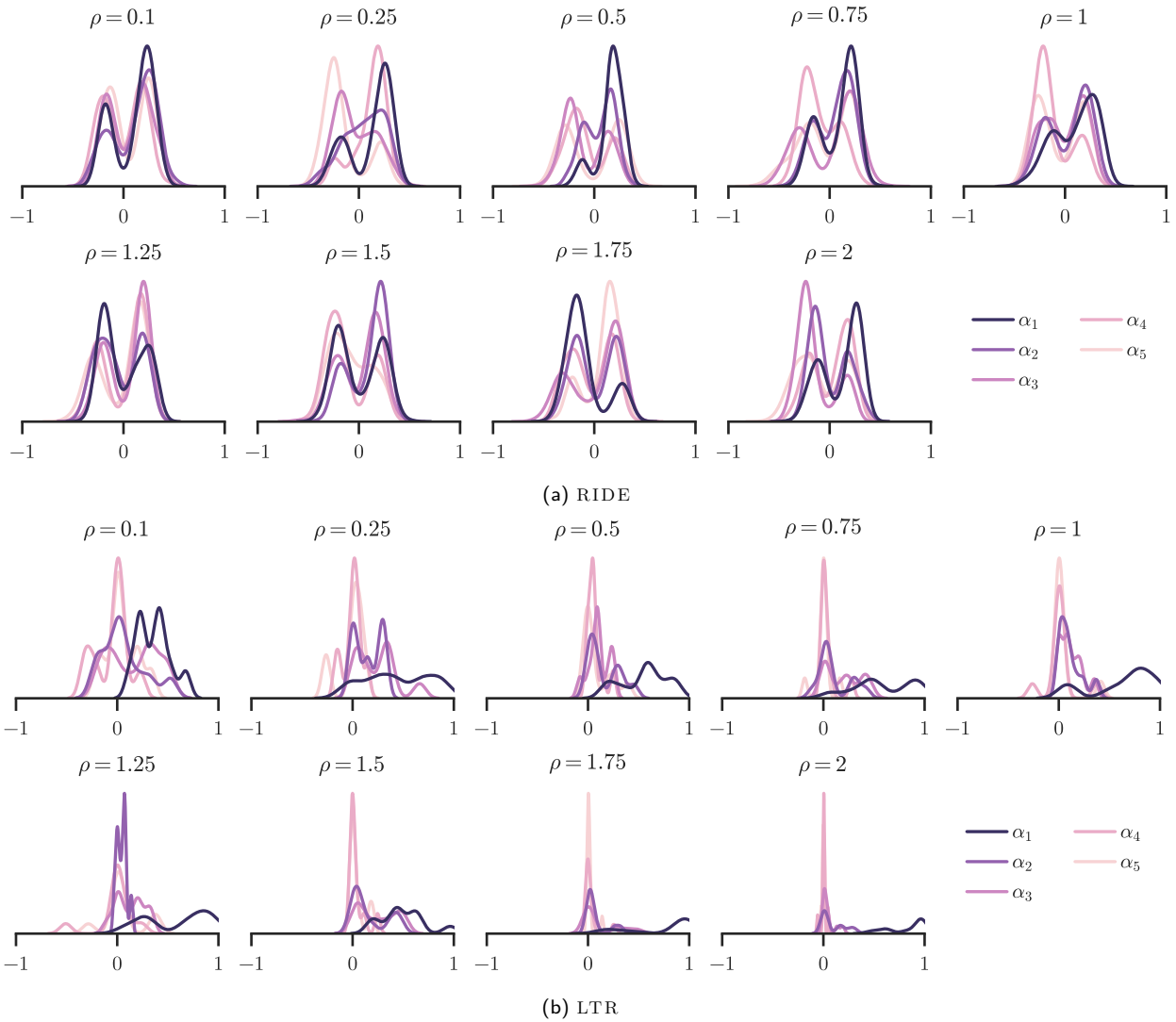


Figure A15: Distribution of α s for AlphaNet trained on CIFAR-100-LT.